

Delamination and ultra-deep subduction of continental crust: constraints from elastic wave velocity and density measurement in ultrahigh-pressure metamorphic rocks

Z. ZHAO,¹ Y. NIU,^{1,2,3} N. I. CHRISTENSEN,⁴ W. ZHOU,⁵ Q. HOU,¹ Z. M. ZHANG,⁶ H. XIE,⁵
Z. C. ZHANG¹ AND J. LIU¹

¹State Key Laboratory of Geological Processes and Mineral Resources and School of Earth Science and Mineral Resources, China University of Geosciences, Beijing 100083, China (zdzhao@cugb.edu.cn)

²School of Earth Sciences, Lanzhou University, Lanzhou 730000, China

³Department of Earth Sciences, Durham University, Durham DH1 3LE, UK

⁴Department of Earth and Ocean Sciences, University of British Columbia, Vancouver, BC V7C3W2, Canada

⁵Institute of Geochemistry, Chinese Academy of Sciences, Guiyang 550002, China

⁶Institute of Geology, Chinese Academy of Geological Sciences, Beijing 100029, China

ABSTRACT Thirty-three samples, including 22 eclogites, collected from the Dabie ultrahigh-pressure (UHP) metamorphic belt in eastern China, have been studied for seismic properties. Compressional (V_p) and shear wave (V_s) velocities in three mutually perpendicular directions under hydrostatic pressures up to 1.0 GPa were measured for each sample. At 1.0 GPa, V_p (7.5–8.4 km s⁻¹), V_s (4.2–4.8 km s⁻¹), and densities (3.2–3.6 g cm⁻³) in the UHP eclogites are higher than those of UHP orthopyroxenite (7.3–7.5 km s⁻¹, 4.1–4.3 km s⁻¹, 3.2–3.3 g cm⁻³, respectively) and HP eclogites (7.1–7.9 km s⁻¹, 4.0–4.5 km s⁻¹, 3.1–3.5 g cm⁻³, respectively). Kyanites (with 99.5% kyanite) show extremely high velocities and density (9.37 km s⁻¹, 5.437 km s⁻¹, 3.581 g cm⁻³, respectively). The eclogites show variation of V_p - and V_s -anisotropy up to 9.70% and 9.17%, respectively. Poisson's ratio (σ) ranges from 0.218 to 0.278 (with a mean of 0.255) for eclogites, 0.281–0.298 for granulites and 0.248 to 0.255 for amphibolites. The σ values for serpentinite (0.341) and marble (0.321) are higher than for other lithologies. The elastic moduli K , G , E of kyanite were obtained as 163, 102 and 253 GPa, respectively. The V_p and density of representative UHP metamorphic rocks (eclogite & kyanite) were extrapolated to mantle depth (15 GPa) following a reasonable geotherm, and compared to the one dimension mantle velocity and density model. The comparison shows that V_p and density in eclogite and kyanite are greater than those of the ambient mantle, with differences of up to $\Delta V_p > 0.3$ km s⁻¹ and $\Delta \rho > 0.3$ –0.4 g cm⁻³, respectively. This result favours the density-induced delamination model and also provides evidence in support of distinguishing subducted high velocity materials in the upper mantle by means of seismic tomography. Such ultra-deep subduction and delamination processes have been recognized by seismic tomography and geochemical tracing in the postcollisional magmatism in the Dabie region.

Key words: Dabie; delamination; eclogite; elastic wave velocity; subduction.

INTRODUCTION

The Dabie–Sulu ultra-high pressure metamorphic (UHPM) belt in eastern China is one of the type UHPM terranes known on Earth. Since the recognition of coesite and micro-diamond inclusions in the 1980s (e.g. Okay *et al.*, 1989; Wang *et al.*, 1989; Xu *et al.*, 1992), much research on the geology, geochemistry, geochronology and geophysics has been carried out on the Dabie–Sulu UHPM belt (see the review by Zheng *et al.*, 2003 and references therein). Physical

properties of the UHP eclogite have also been studied in the past decade, especially on drill core samples recovered from the Chinese Continental Scientific Drilling Project (CCSD) in Donghai, Jiangsu province. These petro-physical results of high-pressure metamorphic (HPM) and UHPM samples from both surface outcrops and drill cores were well-correlated with the deep seismic data (Wang *et al.*, 1997, 2000, 2005a,b; Kern *et al.*, 1999, 2002; Gao *et al.*, 2001; Ji *et al.*, 2003, 2007, 2009; Yang, 2009), thus providing constraints on the nature and compositions of the lower crust and upper mantle beneath the Dabie–Sulu UHPM belt. The seismic velocity measurements by Kern *et al.* (1999, 2002) and Gao *et al.* (2001) were carried out on the cubic samples without jacket

Re-use of this article is permitted in accordance with the Terms and Conditions set out at http://wileyonlinelibrary.com/onlineopen#OnlineOpen_Terms

treatment at pressures up to 600 MPa, which could not fully characterize the intrinsic properties of these very hard UHPM rocks under hydrostatic conditions as pointed out by the authors themselves. The more recent studies (e.g. Ji *et al.*, 2003, 2007, 2009; Wang *et al.*, 2005a,b) have, to some extent, overcome this short-coming and measured the P- and S-wave velocities on samples of varying lithologies from the Dabie–Sulu HPM/UHPM Belt under purely hydrostatic pressures up to 800 MPa.

In this paper, new measurements on P- and S-wave velocities at hydrostatic pressures up to 1000 MPa (1.0 GPa) and densities at the ambient condition are presented for 33 samples collected from the Dabie HPM/UHPM belt. In particular, we show properties of kyanite that has a very high wave velocity ($V_p = 9.37 \text{ km s}^{-1}$, $V_s = 5.437 \text{ km s}^{-1}$ at 1000 MPa) with much lower V_p and V_s pressure derivatives. Using these new findings together with the literature data, we carefully select suitable parameters for extrapolating densities and elastic wave velocities of the UHPM rocks to mantle depths and discuss their implications for deeply subducted continental materials.

GEOLOGICAL SETTING AND SAMPLING

Dabie–Sulu orogen is the central part of the Qinling–Tongbai–Dabie–Sulu orogenic belt in eastern China, resulting from the continental collision between the North China and Yangtze cratons in the Triassic (245 to 210 Ma) indicated by the peak UHPM ages. The Dabie–Sulu UHPM belt has been a global attraction since the recognition of coesite and diamond inclusions and other lines of evidence for UHPM in 1980s because they indicate that the host rocks must have subducted to mantle depths of > 120–200 km before subsequent exhumation along with mantle rocks (e.g. Okay *et al.*, 1989; Wang *et al.*, 1989; Xu *et al.*, 1992; Yang *et al.*, 1993; Liou *et al.*, 1997; Ye *et al.*, 2000). Later research demonstrates that the Dabie–Sulu UHP massif, tens of kilometres in width and hundreds of kilometres in length, has retained coherency during subduction and exhumation, representing one of the largest UHPM belts on Earth (Zheng *et al.*, 2003 and references therein). There has been much research on the geochronology, metamorphic geology, geochemistry, and all aspects of the UHPM rocks as well as geodynamics of the orogen (see Zheng *et al.*, 2003; Ernst & Liou, 2008; Liou *et al.*, 2009 for review). Moreover, deep geophysical survey and CCSD have also been done in the region, which provided unprecedented data on the deep structure of the UHPM belt (e.g. Wang *et al.*, 1997, 2000; Zhang *et al.*, 2000; Yang, 2009).

Generally, the Dabie orogen is divided into four major tectonic units from south to north (Fig. 1; You *et al.*, 1996): (I) Ankang–Wudang massif without HPM and UHPM rocks; (II) South Qinling–Tongbai–Dabie high pressure (HP) and UHPM terrane; (III) The UHPM terrane in Qinling, extending to the north-

western Dabie; (IV) The North Qinling and North Huaiyang terranes. The Dabie HP and UHP terrane (II) is further divided into five subunits: epidote blueschist belt (II–1), HP/Low temperature (LT) eclogite belt (II–2), UHP eclogite belt (II–3), HP/Medium temperature (MT) eclogite belt (II–4) and belt without eclogite (II–5). Among them, the UHP eclogite belt (II–3) is termed as Central Dabie, composed of eclogites, gneisses and marbles, where diamond and coesite inclusions were reported. The eclogites in II–3, occurring as lenses, vary in size from a few centimetres to over a kilometre in length enclosed in the host gneisses. Despite detailed HPM/UHPM studies in a number of localities, the overall P – T – t paths of the Dabie–Sulu HP/UHP belt remain qualitatively as generalized in Fig. 2 (also see Zheng *et al.*, 2003).

Our 33 samples were collected from II–5 (three granulite) and HP/LT (II–2), UHP (II–3) and HP/MT (II–4) eclogite belts (22 HP/UHP eclogites, one UHP kyanite, one UHP orthopyroxene, two amphibolite, 1 serpentinite, 1 garnet-bearing phengite schist, one jadeite quartzite & one marble) (Table 1), and have been studied petrologically (e.g. You *et al.*, 1996), except for the kyanite and jadeite quartzite samples.

SAMPLES AND EXPERIMENTAL TECHNIQUE

A full description of sample localities, rock types, mineral modes and major element compositions are detailed in Tables 1 & 2. The bulk-rock major element analysis was done by wet chemistry method at the Institute of Geochemistry, Chinese Academy of Sciences. The precision and accuracy are better than 5% (Zhao *et al.*, 1998). The density (ρ), compressional wave velocity (V_p), and shear wave velocity (V_s) measurements were all made in the Department of Geology and Geophysics, University of Wisconsin at Madison, USA. Measurements on three mutually perpendicular directions (λ , for banded and foliated rocks, X parallel to lineation, Y perpendicular to lineation and Z normal to foliation) were taken for each sample using a diamond-coring bit with 2.54 cm diameter. Each core sample is ~ 5 cm in length with the core ends ground flat and parallel to within 0.07 cm. The density of each core was calculated from their weights and dimensions at the ambient condition assuming no porosity. Each core was then fitted with a soldered copper jacket to prevent penetration of high-pressure fluid into the rock samples. The high-pressure fluid used was plexol, produced by Esso Corporation. One megahertz transducer was affixed to both core ends when making velocity measurements. Gum rubber tubing was placed over the sample assembly for further prevention of possible oil leakage. Velocities (V_p & V_s) were measured at room temperature under hydrostatic pressures of up to 1000 MPa (1.0 GPa) (equivalent to ~ 35 km depth) using the pulse transmission technique (Christensen, 1985). The cumulative error limits for V_p and V_s were estimated to be > 1%.

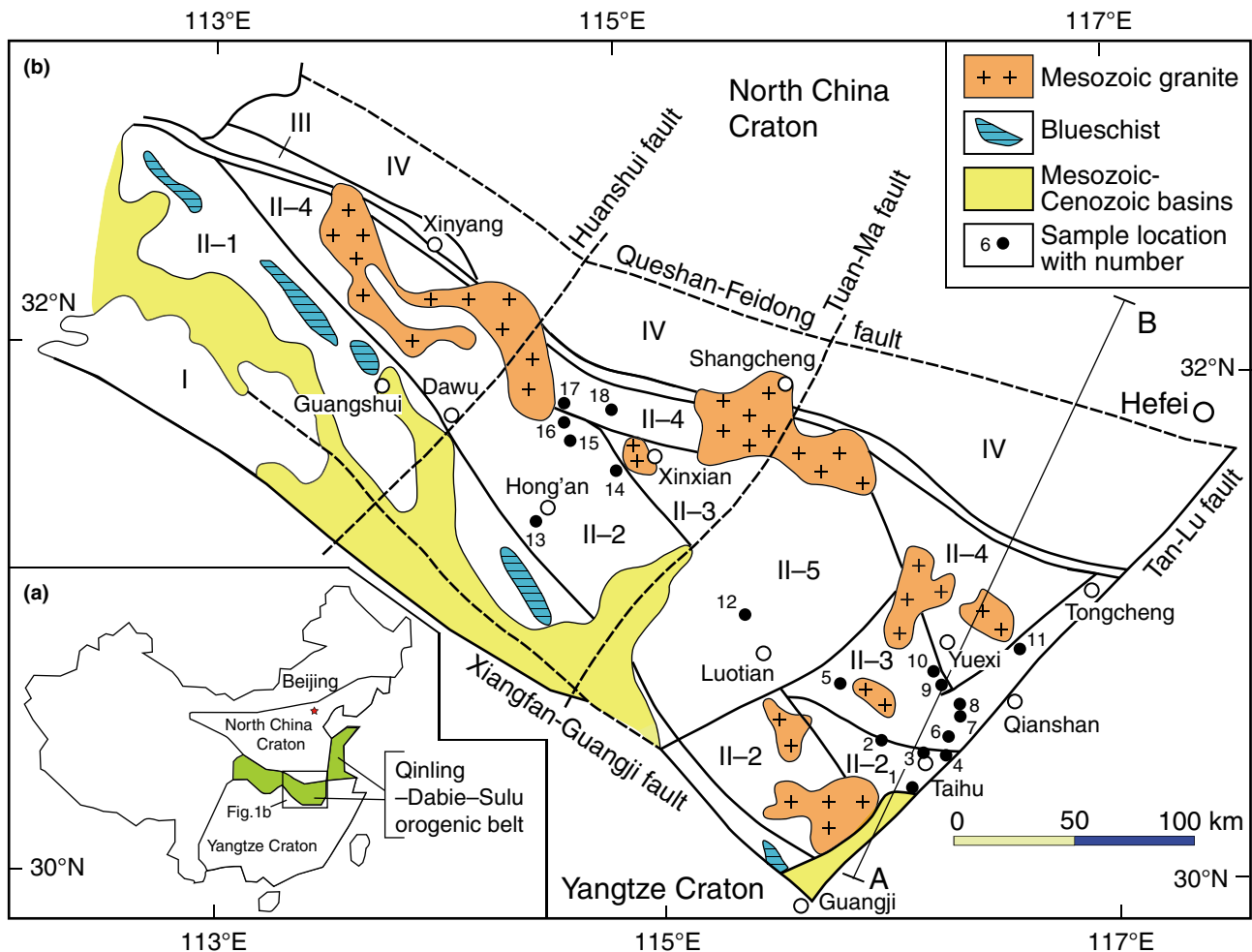


Fig. 1. Simplified geological map of the Dabie ultrahigh-pressure (UHP) metamorphic belt with sample localities, eastern China (modified from You *et al.*, 1996). The main tectonic units are: I, Ankang–Wudang massif; II, South Qinling–Tongbai–Dabie high pressure (HP) and UHP metamorphic terrane; II-1, Epidote blueschist belt; II-2, HP/Low temperature (LT) eclogite belt; II-3, UHP eclogite belt; II-4, HP/Medium temperature (MT) eclogite belt; II-5, Belt bare of eclogite; III, The UHP metamorphic terrane in Qinling; IV, The North Qinling and North Huaiyang terrane. A–B, location of the seismic profile (Wang *et al.*, 1997, 2000). Sampling localities: 1. Liangtinghe, Susong, 2. Huangzhen, Taihu, 3. Zhujiachong, Taihu, 4. Maowu, Taihu, 5. Bamaojie, Yingshan, 6. Shima, Taihu, 7. Shuanghe, Qianshan, 8. Mayuan, Qianshan, 9. Wumiao, Qianshan, 10. Bixiling, Qianshan, 11. Yuantan, Qianshan, 12. Huilanshan, Luotian, 13. Gaoqiao, Hong'an, 14. Chendian, Xinxian, 15. Luwang, Dawu, 16. Xuanhuadian, Dawu, 17. Xiongjian, Qianshan, 18. Qianjinhepeng, Xinxian.

Readings were taken at intervals of 20 MPa in the range of 0–200 MPa, and then at intervals of 200 MPa in the range of 200–1000 MPa.

RESULTS

V_p and V_s variation with pressures

V_p and V_s of the 33 samples (three directions in each sample, except for MW01-3 in one direction) at pressures up to 1000 MPa were obtained. The experimental results and related calculations were given in Table 3. The V_p and V_s in three representative samples (kyanite, eclogite & granulite) were plotted in Fig. 3. The V_p and V_s increase quickly with increasing pressure in the range of 0–300 MPa, increase slowly between 300 and

1000 MPa, and exhibit a linear trend for both V_p and V_s with increasing pressure from 400 to 1000 MPa for most of the samples. The closure pressure of microfractures in these rocks is ~300 MPa, which is similar to the results at pressures up to 600 MPa (Kern *et al.*, 1999, 2002; Gao *et al.*, 2001) and 800 MPa (Wang *et al.*, 2005a,b; Ji *et al.*, 2007), but lower than that under higher pressures up to 3–5 GPa (Matsushima, 1972; Christensen, 1974; Zhao *et al.*, 1998, 1999). Pressure derivatives of V_p (dV_p/dP) and V_s (dV_s/dP) (in $10^{-4} \text{ km s}^{-1} \text{ MPa}^{-1}$) are calculated from the linear part of 600–1000 MPa by least-square fit to obtain the linear functions. The best linear relationship between wave velocity and pressure is in the range of 600–1000 MPa with $R^2 \geq 0.99$ in most of the samples (Table 3). The majority of the dV_p/dP and dV_s/dP

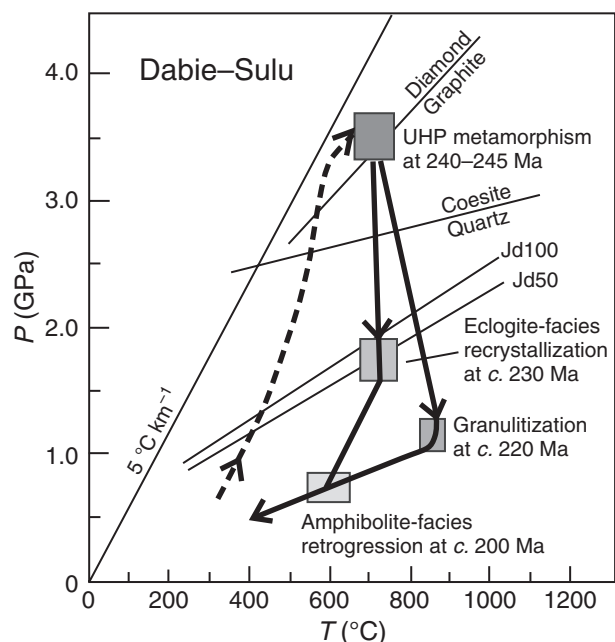


Fig. 2. Schematic P - T - t diagram showing the differential uplifts of different two-stage processes for the UHP eclogite facies rocks in Dabie UHPM belt (Zheng *et al.*, 2003).

values obtained in this work are less than $2 \times 10^{-4} \text{ km s}^{-1} \text{ MPa}^{-1}$, with averages of 1.415 and $0.627 \times 10^{-4} \text{ km s}^{-1} \text{ MPa}^{-1}$, respectively (Fig. 4).

V_p and V_s against density and chemistry

The V_p and V_s of different lithologies at 1000 MPa as a function of zero-pressure densities are plotted in Fig. 5a,b. All the data show a first-order positive linear trend (Fig. 5a,b). The UHP eclogite ($N = 12$) have, on average, higher V_p (7.5–8.4 km s^{-1}), V_s (4.2–4.8 km s^{-1}) and ρ (3.2–3.6 g cm^{-3}) than the UHP orthopyroxenite ($N = 2$, $V_p = 7.3$ –7.5 km s^{-1} , $V_s = 4.1$ –4.3 km s^{-1} , $\rho = 3.2$ –3.3 g cm^{-3}) and HP eclogites ($N = 9$, $V_p = 7.1$ –7.9 km s^{-1} , $V_s = 4.0$ –4.5 km s^{-1} , $\rho = 3.1$ –3.5 g cm^{-3}). The density and V_p and V_s of HP garnet-bearing granulite and amphibolites overlap, but are higher than the lower-grade metamorphic rocks (Fig. 5a,b). Serpentinites have the lowest values for these parameters. Also measured for the first time are the seismic properties of kyanite (sample LJ01-1, with 99.5% kyanite & 0.5% corundum), which has the highest wave velocities ($V_p = 9.37 \text{ km s}^{-1}$, $V_s = 5.437 \text{ km s}^{-1}$ at 1.0 GPa) and density (3.581 g cm^{-3}). Bulk-rock SiO_2 against V_p were plotted in Fig. 5c. There

Table 1. Sample localities, rock type and modal compositions.

No.	Sample	Locality and number ^a	Lithology	Modal compositions (%)
1	BM961	Bamaojie, Yingshan, 5	Fine-grained coesite-bearing eclogite	Grt 35, Cpx 25, Hbl 15, Pl 10, Ms 5, Qtz 5, (Ap, Rt) 5
2	BX01-2	Bixiling, Qianshan, 10	Fine-grained phengite eclogite	Grt 35, Cpx 14, Qtz 14, Phn 7, Hbl 2, Rt 2, Symp 26
3	BX01-5	Bixiling, Qianshan, 10	Medium-grained eclogite	Grt 35, Cpx 44, Zo 14, Qtz 5, Rt 2
4	BX01-6	Bixiling, Qianshan, 10	Pyroxene amphibolite	Hbl 47, Cpx 30, Zo 13, Chl 6, Pl 3, Rt 1
5	BX962	Bixiling, Qianshan, 10	Fine-grained phengite eclogite	Grt 35, Cpx 25, Qtz 10, Hbl 2, Rt 2, Symp 26
6	CD-962	Chendian, Xinxian, 14	Eclogite	Grt 45, Cpx 35, Hbl 10, (Ms, Mt, Ep, Rt, Qtz) 10
7	GQ961	Gaoqiao, Hong'an, 13	Eclogite	Grt 35, Hbl 40, Gln 10, Cc 10, Ms 3, Qtz, 1, Mt 1
8	HL963	Huilanshan, Luotian, 12	Granulite	Pl 55, Bi 20, Cpx 10, Opx 5, Hbl 5, Mt 2, Qtz 2, Ap 1
9	HL968	Huilanshan, Luotian, 12	Fine-grained granulite	Pl 47, Cpx 28, Opx 12, Hbl 8, Mt 5
10	HL969	Huilanshan, Luotian, 12	Granulite	Pl 45, Cpx 40, Opx 5, Hbl 5, Bi 3, Mt 1, Qtz 1
11	HZ964	Huangzhen, Taihu, 2	Retrogressed eclogite	Grt 24, Cpx 48, Hbl 8, Bi 5, Ms 6, Zo 4, Rt 2, Qtz 3
12	HZ967	Huangzhen, Taihu, 2	Retrogressed eclogite	Grt 35, Cpx 44, Hbl 6, Ms 8, Qtz 2, Rt 1, Zo 4
13	LJ01-1	Liangtinghe, Susong, 1	Kyanite	Ky 99.5, Crn 0.5
14	LW961	Luwang, Dawu, 15	Fine-grained marble	Cc 98, Qtz 1.5, Ms 0.5
15	LW965	Luwang, Dawu, 15	Serpentinite	Srp 93, Mt 5, Ol 2
16	MW01-1	Maowu, Taihu, 4	Fine-grained eclogite	Grt 40, Cpx 58, Rt 2
17	MW01-2	Maowu, Taihu, 4	Eclogite	Grt 30, Cpx 68, Rt 2
18	MW01-3	Maowu, Taihu, 4	Garnet-bearing orthopyroxenite	Opx 65, Cpx 30, Grt 10
19	MY01-3	Mayuan, Qianshan, 8	Garnet-bearing phengite schist	Grt 24, Phn 36, Bi 8, Qtz 29, Ky 2, Rt 1
20	QJ961	Qianjinhepeng, Xinxian, 18	Garnet amphibolite	Grt 35, Hbl 45, Qtz 10, Pl 3, Spn 5, Mt 1, Ep 1
22	SH965	Shuanghe, Qianshan, 7	Medium-grained coesite-bearing eclogite	Grt 51, Cpx 24, Qtz 12, Cc 3, Rt 2, Symp 8
24	SH966	Shuanghe, Qianshan, 7	Medium-grained jadeite quartzite	Qtz 58, Jd 39, Grt 4.5, Gln 0.5
26	SH967	Shuanghe, Qianshan, 7	Eclogite	Grt 40, Hbl 25, Cpx 10, Ep 10, Ms 10, (Rt, Zo, Ap) 5
24	SM961	Shima, Taihu, 6	Coesite-bearing eclogite	Grt 40, Cpx 55, Hbl 2, Rt 1, Mt 1, Qtz 1
25	SM962	Shima, Taihu, 6	Medium-grained eclogite	Grt 35, Cpx 25, Zo 15, Qtz 12, Rt 1, Symp 12
26	SM969	Shima, Taihu, 6	Fine-grained eclogite	Grt 52, Cpx 46, Rt 2
27	WM962	Wumiao, Qianshan, 9	Coesite-bearing eclogite	Grt 45, Cpx 45, (Hbl, Ms, Mt, Ep, Rt, Qtz) 10
28	XD01-1	Xiongdian, Qianshan, 17	Eclogite	Grt 40, Cpx 40, Hbl 10, Ms 6, Qtz 2, Rt 2
29	XD962	Xiongdian, Qianshan, 17	Eclogite	Grt 45, Cpx 35, Hbl 10, Ep 5, Qtz 3, (Rt, Ms, Ap, Ttn) 2
30	XD966	Xiongdian, Qianshan, 17	Eclogite	Grt 38, Cpx 30, Hbl 20, Ep 7, Qtz 3, (Rt, Ap, Cc) 2
31	XH961	Xuanhuadian, Dawu, 16	Eclogite	Grt 25, Tr 35, Zo 20, Cpx 10, Ms 5, Rt 3, Mt 2
32	YT963	Yuantan, Qianshan, 11	Fine-grained eclogite	Grt 46, Cpx 41, Qtz 4, Rt 1, Symp 8
33	ZJ01-1	Zhujiachong, Taihu, 3	Medium-grained eclogite	Grt 26, Jd 40, Cpx 7, Zo 15, Ms 3.5, Qtz 0.5, Symp 8

^aSample locality numbers are the same as in Fig. 1.

Ap, apatite; Bi, biotite; Cc, calcite; Chl, chlorite; Crn, corundum; Ep, epidote; Gln, glaucophane; Grt, garnet; Hbl, hornblende; Jd, jadeite; Ky, kyanite; Ms = muscovite; Mt, magnetite; Ol, olivine; Opx, orthopyroxene; Phn, phengite; Pl, plagioclase; Qtz, quartz; Rt, rutile; Srp, serpentine; Symp, symplectite; Tr, tremolite; Ttn, titanite; Zo, zoisite.

Table 2. Bulk-rock compositions (wt%).

Sample	SiO ₂	TiO ₂	Al ₂ O ₃	Fe ₂ O ₃	FeO	MnO	MgO	CaO	Na ₂ O	K ₂ O	H ₂ O ⁺	H ₂ O ⁻	P ₂ O ₅	CO ₂	Total
BM961	49.98	1.53	11.57	12.45	5.55	0.40	4.20	8.20	2.72	0.01	0.42	0.02	0.71	1.43	99.19
BX01-2	52.67	0.28	16.15	7.81	3.77	0.32	3.90	7.90	3.92	0.57	0.28	0.07	0.73	0.94	99.31
BX01-5	50.71	0.07	15.91	5.42	2.41	0.17	8.90	12.90	1.33	0.08	0.25	0.16	0.11	0.70	99.12
BX01-6	47.05	0.13	20.72	3.87	4.62	0.17	9.90	8.90	1.92	0.15	1.14	0.07	0.15	0.46	99.26
BX962	51.77	0.06	19.82	3.43	4.67	0.14	5.60	8.60	1.75	0.14	1.15	0.10	0.06	1.80	99.09
CD962	50.44	0.31	14.77	12.45	1.75	0.28	3.90	7.60	3.85	0.24	1.73	0.07	0.33	1.49	99.21
GQ961	43.38	0.47	10.60	14.36	6.24	0.28	6.30	8.90	2.10	0.03	2.80	0.13	0.12	3.61	99.32
HL963	50.13	1.15	17.35	6.20	4.60	0.16	4.90	6.90	3.93	1.91	0.62	0.03	0.80	1.01	99.69
HL968	44.92	1.94	15.16	11.66	9.04	0.27	4.80	7.00	2.75	0.39	0.10	0.01	0.51	0.99	99.54
HL969	43.46	1.67	13.73	12.07	8.73	0.39	5.20	9.10	2.28	0.59	0.90	0.05	0.41	1.04	99.62
HZ964	49.71	0.67	16.60	9.13	3.77	0.18	4.60	6.40	4.01	0.92	0.95	0.10	0.40	2.00	99.44
HZ967	46.85	0.34	17.35	7.52	4.28	0.33	7.50	7.70	3.55	1.29	0.63	0.05	0.29	1.87	99.55
LJ01-1	36.11	0.10	61.05	1.06	0.08	0.02	0.10	0.10	0.03	0.03	1.21	0.23	0.10	0.00	100.22
LW961	2.87	0.06	0.04	0.06	0.17	0.01	1.00	54.30	0.05	0.01	0.70	0.05	0.05	40.10	99.47
LW965	32.60	0.01	1.44	4.30	2.10	0.14	38.80	1.80	0.37	0.08	12.70	0.32	0.03	5.03	99.72
MW01-1	48.19	0.13	11.57	5.02	6.10	0.25	9.70	15.30	1.32	0.00	0.21	0.07	0.23	1.09	99.18
MW01-2	45.31	0.64	11.09	4.50	4.59	0.26	14.60	15.60	0.18	0.00	0.28	0.09	0.75	1.26	99.15
MW01-3	52.05	0.05	5.78	4.58	3.44	0.19	28.90	1.90	0.03	0.01	0.89	0.10	0.29	1.25	99.46
MY01-3	57.64	0.31	19.04	4.22	3.04	0.22	3.90	3.10	1.27	4.03	0.64	0.10	0.09	1.43	99.03
QJ961	47.78	1.53	12.53	8.40	10.40	0.29	4.80	8.50	2.33	0.47	0.84	0.05	0.23	0.97	99.12
SH965	54.10	0.41	13.56	10.76	5.14	0.19	4.00	5.50	1.73	0.03	0.70	0.09	0.30	2.70	99.21
SH966	71.31	0.14	14.26	4.47	1.33	0.07	1.00	1.10	5.30	0.24	0.69	0.05	0.09	-	100.05
SH967	41.27	0.27	17.09	13.30	5.20	0.29	6.20	11.00	1.98	0.17	0.22	0.03	1.41	1.09	99.52
SM961	42.41	0.35	12.53	15.29	5.01	0.39	5.10	11.20	2.89	0.02	0.49	0.03	1.47	1.92	99.10
SM962	53.93	0.09	14.94	5.81	2.69	0.18	5.70	11.50	1.44	0.05	0.73	0.07	0.13	1.90	99.16
SM969	49.26	0.09	18.25	7.39	3.11	0.21	8.70	6.90	2.16	0.02	1.10	0.15	0.07	1.75	99.16
WM962	50.21	0.07	14.21	7.42	2.88	0.20	7.90	10.70	2.90	0.25	0.92	0.09	0.07	1.36	99.18
XD01-1	47.84	0.11	16.38	5.18	3.35	0.18	7.60	11.30	2.59	0.74	1.14	0.08	0.11	2.68	99.28
XD962	45.03	0.33	16.87	10.06	9.04	0.26	3.90	11.00	1.86	0.09	0.60	0.03	0.11	0.70	99.88
XD966	43.66	0.42	14.21	5.79	4.41	0.25	6.00	16.30	1.11	0.14	3.09	0.30	0.12	3.30	99.10
XH961	47.28	0.25	16.62	7.12	4.98	0.20	7.80	9.10	2.61	0.48	1.32	0.10	0.21	1.06	99.13
YT963	45.70	1.19	16.36	10.00	7.89	0.23	5.60	7.70	2.39	0.03	0.71	0.06	0.52	0.67	99.05
ZJ01-1	49.07	0.36	17.11	4.69	4.60	0.21	6.50	10.00	3.98	0.07	0.31	0.08	0.29	2.16	99.43

is a weak V_p decrease with increasing SiO₂. For rocks of mafic protoliths, V_p increases with increasing metamorphic grade from unmetamorphosed rocks, through amphibolite to granulite, and to eclogite.

Anisotropy

Rock velocity anisotropy is an important feature genetically associated with deformation fabrics, including lineation, foliation oriented micro cracks and lattice preferred orientation (LPO) of the minerals in rocks of interest (e.g. Kern & Wenk, 1990; Ji *et al.*, 1993; Kern *et al.*, 1999, 2002). The anisotropy (A) for V_p and V_s can be defined by $A = [(V_{\max} - V_{\min}) / V_{\text{mean}}] \times 100(\%)$ (Birch, 1961), where, in a foliated metamorphic rock, the V_{\max} usually parallels foliation and lineation, V_{\min} is normal to the foliation and lineation, and V_{mean} is the mean velocity in the three mutually perpendicular directions. The V_p -A and V_s -A values of the 33 samples are shown in Fig. 6. In most of the samples, the anisotropy reaches steady values at pressures over 400 MPa, which represents the microfracture-free anisotropy as a result of LPO-related manner. At 1000 MPa, variation of V_p - and V_s -A in the 33 samples is up to 12%. Among them, 22 UHP and HP eclogites yield more variable V_p -A (0.34–9.70%) and V_s -A (0.2–9.17%). The high V_p -A and V_s -A for eclogite sample YT963 (9.70 & 9.17%) is associated with mineralogical layering, and the high

V_p -A and V_s -A for eclogite sample XD966 (6.87 & 8.97%) results from retrograde metamorphism (e.g. ~30% Cpx & 20% Hbl) and foliations. The kyanite has very low V_p -A (0.56%) and V_s -A (1.38%). The anisotropy of eclogite is largely caused by garnet and omphacite layering and foliation. For instance, the lower V_p -A were found in fine- to medium-grained HP and UHP eclogites (e.g. 0.34–0.99%), which are consistent with their lack of foliation and random distribution of varying garnet and omphacite (cpx) modes (24–52% & 40–47%, respectively). In general, a complex relationship exists between rock anisotropy and its microcracks, LPO, mineral constitution at high pressures (Ji *et al.*, 2007).

Poisson's ratios

Poisson's ratio (σ) in rocks is calculated using the following equation:

$$\sigma = \frac{1}{2} \left[1 - \frac{1}{(V_p/V_s)^2 - 1} \right]$$

Since V_p and V_s are nearly constant over 300–400 MPa, the ratio of V_p/V_s and σ at this pressure range already reach intrinsic values, i.e. the same at pressures of 400–1000 MPa (Fig. 7). The V_p and σ variation with lithologies are shown in Fig. 8a. The σ ranges from 0.218 to 0.278 (mean 0.255) in HP and UHP eclogites,

Table 3. Density, P- (V_p) and S-wave (V_s) velocities, anisotropies (A/%) of V_p and V_s , V_p/V_s and Poisson's ratio (σ) measured at pressures up to 1000 MPa of the Dabie samples. Reference velocities (V_{p0} and V_{s0}) and pressure derivatives (D) of V_p and V_s are calculated from the linear relationship between 600 MPa and 1000 MPa.

Samples	V_p, V_s	λ^a	Density (g cm^{-3})	V_p and V_s (km s^{-1}) at Pressures (MPa)										V_p (V_s) = $V_0(V_{p0}/V_{s0}) + DP$			
				20	40	60	80	100	200	400	600	800	1000	V_0 (km s^{-1})	$D(10^{-4} \text{ km s}^{-1} \text{ MPa}^{-1})$	R^2	
UHP eclogite																	
BM961	V_p	X	3.324	6.433	6.680	6.834	6.942	7.021	7.233	7.406	7.504	7.575	7.630	7.318	3.15	0.99	
		Y	3.311	6.127	6.442	6.658	6.817	6.938	7.248	7.434	7.517	7.574	7.619	7.366	2.55	1.00	
		Z	3.307	6.056	6.391	6.615	6.775	6.892	7.174	7.339	7.419	7.476	7.520	7.270	2.52	0.99	
		Mean	3.314	6.205	6.504	6.702	6.845	6.950	7.218	7.393	7.480	7.542	7.590	7.318	2.74		
	V_s	X	3.324	3.806	3.889	3.950	3.997	4.033	4.129	4.177	4.190	4.198	4.204	4.169	0.35	0.99	
		Y	3.311	3.717	3.818	3.891	3.947	3.992	4.115	4.186	4.210	4.224	4.236	4.171	0.65	1.00	
		Z	3.307	3.554	3.727	3.839	3.916	3.969	4.080	4.134	4.159	4.178	4.192	4.110	0.82	0.99	
		Mean	3.314	3.692	3.811	3.893	3.953	3.998	4.108	4.166	4.186	4.200	4.211	4.150	0.61		
	V_p/V_s	σ		1.681	1.707	1.721	1.731	1.738	1.757	1.775	1.787	1.796	1.802				
		σ		0.226	0.239	0.245	0.250	0.253	0.260	0.267	0.272	0.275	0.278				
	BX01-5	V_p	X	3.373	7.181	7.320	7.426	7.512	7.584	7.810	7.972	8.021	8.045	8.061	7.963	0.99	0.99
			Y	3.394	7.054	7.225	7.349	7.447	7.526	7.761	7.918	7.972	8.004	8.028	7.890	1.39	0.99
Z			3.359	7.112	7.261	7.375	7.468	7.543	7.773	7.922	7.964	7.985	8.000	7.912	0.88	0.99	
Mean			3.375	7.116	7.268	7.383	7.475	7.551	7.781	7.937	7.986	8.012	8.030	7.922	1.09		
V_s		X	3.373	4.146	4.248	4.319	4.374	4.417	4.537	4.616	4.648	4.670	4.686	4.592	0.95	0.99	
		Y	3.394	4.121	4.263	4.355	4.421	4.468	4.586	4.662	4.701	4.728	4.750	4.628	1.23	0.99	
		Z	3.359	4.255	4.339	4.401	4.449	4.488	4.598	4.666	4.687	4.700	4.709	4.655	0.54	0.99	
		Mean	3.375	4.174	4.283	4.358	4.414	4.458	4.574	4.648	4.679	4.699	4.715	4.625	0.91		
V_p/V_s		σ		1.705	1.697	1.694	1.693	1.694	1.701	1.708	1.707	1.705	1.703				
		σ		0.238	0.234	0.233	0.232	0.233	0.236	0.239	0.239	0.238	0.237				
BX962		V_p	X	3.384	6.776	6.983	7.133	7.250	7.345	7.626	7.819	7.889	7.932	7.963	7.780	1.85	0.99
			Y	3.389	6.624	6.888	7.082	7.235	7.361	7.736	7.991	8.078	8.129	8.166	7.948	2.20	0.99
	Z		3.354	6.126	6.436	6.660	6.829	6.959	7.297	7.474	7.534	7.573	7.604	7.431	1.74	0.99	
	Mean		3.376	6.509	6.769	6.958	7.105	7.222	7.553	7.761	7.834	7.878	7.911	7.720	1.93		
	V_s	X	3.384	4.157	4.273	4.352	4.411	4.457	4.584	4.672	4.712	4.739	4.760	4.640	1.21	0.99	
		Y	3.389	3.913	4.061	4.160	4.234	4.292	4.456	4.578	4.637	4.678	4.710	4.529	1.83	1.00	
		Z	3.354	3.781	3.917	4.014	4.090	4.152	4.335	4.461	4.509	4.538	4.560	4.433	1.28	0.99	
		Mean	3.376	3.950	4.084	4.175	4.245	4.300	4.458	4.570	4.619	4.652	4.677	4.534	1.44		
	V_p/V_s	σ		1.648	1.658	1.666	1.674	1.679	1.694	1.698	1.696	1.694	1.692				
		σ		0.208	0.214	0.219	0.222	0.225	0.233	0.235	0.234	0.232	0.231				
	MW01-2	V_p	X	3.628	7.726	7.916	8.027	8.096	8.139	8.225	8.277	8.306	8.327	8.343	8.252	0.92	1.00
			Y	3.539	6.935	7.205	7.385	7.516	7.615	7.866	8.025	8.102	8.156	8.198	7.960	2.40	0.99
Z			3.554	7.082	7.287	7.427	7.529	7.604	7.785	7.883	7.927	7.957	7.980	7.848	1.33	0.99	
Mean			3.574	7.248	7.469	7.613	7.714	7.786	7.959	8.062	8.112	8.146	8.174	8.020	1.55		
V_s		X	3.628	4.427	4.478	4.514	4.540	4.560	4.610	4.636	4.646	4.653	4.659	4.629	0.30	0.99	
		Y	3.539	4.024	4.177	4.276	4.344	4.392	4.499	4.560	4.591	4.613	4.630	4.533	0.98	0.99	
		Z	3.554	4.002	4.138	4.224	4.283	4.326	4.430	4.504	4.544	4.573	4.596	4.468	1.29	0.99	
		Mean	3.574	4.151	4.265	4.338	4.389	4.426	4.513	4.567	4.594	4.613	4.628	4.543	0.86		
V_p/V_s		σ		1.746	1.752	1.755	1.757	1.759	1.764	1.765	1.766	1.766	1.766				
		σ		0.256	0.258	0.260	0.261	0.261	0.263	0.264	0.264	0.264	0.264				
MW01-1		V_p	X	3.525	7.711	7.796	7.860	7.911	7.952	8.081	8.171	8.201	8.217	8.229	8.161	0.68	0.99
			Y	3.456	7.540	7.707	7.813	7.885	7.936	8.058	8.139	8.183	8.215	8.239	8.101	1.39	0.99
	Z		3.446	6.980	7.222	7.324	7.435	7.491	7.657	7.782	7.866	7.927	7.974	7.708	2.68	1.00	
	Mean		3.476	7.410	7.575	7.665	7.743	7.793	7.932	8.031	8.084	8.120	8.147	7.990	1.58		
	V_s	X	3.525	4.340	4.466	4.530	4.566	4.588	4.635	4.676	4.699	4.716	4.729	4.655	0.75	0.99	
		Y	3.456	4.335	4.447	4.504	4.537	4.557	4.601	4.638	4.660	4.675	4.687	4.619	0.69	0.99	
		Z	3.446	4.102	4.210	4.277	4.324	4.358	4.444	4.511	4.548	4.574	4.595	4.478	1.18	0.99	
		Mean	3.476	4.259	4.374	4.437	4.475	4.501	4.560	4.608	4.636	4.655	4.670	4.584	0.87		
	V_p/V_s	σ		1.740	1.732	1.728	1.730	1.732	1.739	1.743	1.744	1.744	1.744				
		σ		0.253	0.250	0.248	0.249	0.250	0.253	0.255	0.255	0.255	0.255				
	SH965	V_p	X	3.409	7.480	7.525	7.554	7.576	7.594	7.652	7.707	7.734	7.752	7.764	7.760	0.75	0.99
			Y	3.397	7.336	7.417	7.461	7.489	7.506	7.548	7.582	7.602	7.617	7.628	7.565	0.63	0.98
Z			3.361	7.239	7.412	7.489	7.525	7.546	7.587	7.623	7.644	7.659	7.671	7.605	0.67	0.99	
Mean			3.389	7.352	7.451	7.501	7.530	7.549	7.596	7.638	7.660	7.676	7.688	7.643	0.68		
V_s		X	3.409	4.276	4.362	4.405	4.428	4.440	4.459	4.469	4.475	4.479	4.483	4.464	0.19	0.99	
		Y	3.397	4.328	4.363	4.387	4.404	4.418	4.454	4.475	4.483	4.489	4.494	4.468	0.26	0.99	
		Z	3.361	4.237	4.293	4.329	4.355	4.372	4.408	4.423	4.429	4.433	4.437	4.418	0.19	0.99	
		Mean	3.389	4.276	4.362	4.405	4.428	4.440	4.459	4.469	4.475	4.479	4.483	4.464	0.19	0.99	

Table 3. (Continued).

Samples	V_p, V_s	λ^a	Density (g cm ⁻³)	V_p and V_s (km s ⁻¹) at Pressures (MPa)										$V_p (V_s) = V_0(V_{p0}/V_{s0}) + DP$			
				20	40	60	80	100	200	400	600	800	1000	V_0 (km s ⁻¹)	$D(10^{-4}$ km s ⁻¹ MPa ⁻¹)	R^2	
SH967	V_p/V_s	σ		1.717	1.717	1.715	1.713	1.712	1.711	1.714	1.717	1.718	1.719				
				0.244	0.243	0.242	0.242	0.241	0.240	0.242	0.243	0.244	0.244				
	V_p	X		3.543	7.028	7.223	7.378	7.501	7.601	7.877	8.014	8.039	8.048	8.054	8.017	0.38	0.99
				3.458	6.488	6.862	7.125	7.320	7.467	7.834	8.022	8.094	8.142	8.180	7.967	2.15	1.00
		Z		3.501	6.839	7.091	7.258	7.380	7.474	7.733	7.923	8.020	8.088	8.141	7.841	3.03	0.99
				3.501	6.785	7.059	7.254	7.400	7.514	7.815	7.986	8.051	8.093	8.125	7.942	1.85	
		A			2.786	1.870	1.654	1.635	1.690	1.843	1.139	0.236	0.494	1.071			
				3.543	4.212	4.283	4.337	4.380	4.415	4.517	4.579	4.596	4.606	4.612	4.573	0.40	0.98
		Y		3.458	3.841	3.968	4.060	4.129	4.183	4.326	4.402	4.428	4.445	4.458	4.516	0.53	
				3.501	4.117	4.205	4.269	4.318	4.358	4.466	4.528	4.547	4.559	4.568	4.384	0.75	0.99
		$Mean$		3.501	4.057	4.152	4.222	4.276	4.319	4.436	4.503	4.524	4.537	4.546	4.491	0.56	
					9.145	7.587	6.561	5.870	5.372	4.305	3.931	3.714	3.549	3.388			
SM961	V_p/V_s	σ		1.673	1.700	1.718	1.731	1.740	1.762	1.774	1.780	1.784	1.787				
				0.222	0.235	0.244	0.249	0.253	0.262	0.267	0.269	0.271	0.272				
	V_p	X		3.627	7.471	7.802	7.977	8.073	8.127	8.209	8.249	8.271	8.287	8.299	8.230	0.70	0.99
				3.587	7.551	7.792	7.937	8.028	8.086	8.188	8.230	8.252	8.267	8.279	8.212	0.68	1.00
		Z		3.558	7.510	7.646	7.737	7.800	7.846	7.954	8.015	8.044	8.064	8.080	7.991	0.90	1.00
				3.591	7.511	7.747	7.884	7.967	8.020	8.117	8.165	8.189	8.206	8.219	8.144	0.76	
		A			0.519	2.014	3.044	3.427	3.504	3.142	2.866	2.772	2.718	2.664			
				3.627	4.341	4.430	4.474	4.498	4.512	4.535	4.552	4.561	4.568	4.573	4.543	0.30	0.99
		Y		3.587	4.349	4.430	4.475	4.501	4.516	4.542	4.557	4.565	4.571	4.576	4.549	0.28	1.00
				3.558	4.385	4.418	4.443	4.462	4.477	4.518	4.543	4.552	4.557	4.561	4.539	0.23	1.00
		$Mean$		3.591	4.358	4.426	4.464	4.487	4.502	4.532	4.551	4.559	4.565	4.570	4.544	0.27	
					1.010	0.271	0.694	0.802	0.777	0.375	0.198	0.197	0.241	0.263			
SM962	V_p/V_s	σ		1.723	1.750	1.766	1.776	1.781	1.791	1.794	1.796	1.797	1.799				
				0.246	0.258	0.264	0.268	0.270	0.274	0.275	0.275	0.276	0.276				
	V_p	X		3.241	6.360	6.560	6.719	6.849	6.958	7.284	7.484	7.530	7.547	7.558	7.488	0.71	0.98
				3.210	6.028	6.297	6.492	6.642	6.761	7.091	7.289	7.358	7.402	7.436	7.244	1.94	0.99
		Z		3.199	6.050	6.284	6.462	6.606	6.723	7.074	7.295	7.358	7.390	7.412	7.279	1.34	0.99
				3.217	6.146	6.380	6.558	6.699	6.814	7.150	7.356	7.415	7.446	7.469	7.337	1.33	
		A			5.048	4.328	3.914	3.638	3.439	2.939	2.559	2.311	2.114	1.954			
				3.241	3.792	3.925	4.020	4.092	4.149	4.306	4.401	4.436	4.459	4.476	4.376	1.01	0.99
		Y		3.210	3.666	3.809	3.912	3.992	4.053	4.215	4.301	4.330	4.348	4.362	4.282	0.81	0.99
				3.199	3.698	3.834	3.934	4.013	4.076	4.255	4.362	4.395	4.415	4.430	4.344	0.86	0.99
		$Mean$		3.217	3.719	3.856	3.955	4.032	4.093	4.259	4.355	4.387	4.407	4.423	4.334	0.89	
					2.540	2.360	2.172	1.969	1.793	1.198	0.886	0.930	0.988	1.051			
SM969	V_p/V_s	σ		1.653	1.655	1.658	1.661	1.665	1.679	1.689	1.690	1.690	1.689				
				0.211	0.212	0.214	0.216	0.218	0.225	0.230	0.231	0.230	0.230				
	V_p	X		3.574	7.728	7.890	7.997	8.074	8.131	8.273	8.364	8.409	8.441	8.465	8.325	1.42	0.99
				3.551	7.687	7.845	7.960	8.046	8.111	8.267	8.332	8.349	8.360	8.369	8.319	0.50	1.00
		Z		3.608	7.661	7.820	7.933	8.018	8.082	8.243	8.323	8.350	8.368	8.382	8.303	0.79	0.99
				3.578	7.692	7.852	7.964	8.046	8.108	8.261	8.339	8.369	8.389	8.405	8.316	0.90	
		A			0.869	0.894	0.802	0.694	0.601	0.355	0.488	0.701	0.866	0.994			
				3.574	4.582	4.624	4.654	4.676	4.693	4.738	4.765	4.776	4.783	4.788	4.757	0.32	0.99
		Y		3.551	4.397	4.513	4.580	4.621	4.648	4.701	4.734	4.752	4.765	4.775	4.718	0.58	0.99
				3.608	4.323	4.454	4.529	4.575	4.605	4.667	4.710	4.735	4.753	4.767	4.689	0.79	0.99
		$Mean$		3.578	4.434	4.530	4.588	4.624	4.649	4.702	4.736	4.754	4.767	4.777	4.721	0.56	
					5.853	3.759	2.711	2.168	1.883	1.509	1.149	0.847	0.623	0.448			
WM962	V_p/V_s	σ		1.735	1.733	1.736	1.740	1.744	1.757	1.761	1.760	1.760	1.760				
				0.251	0.251	0.252	0.253	0.255	0.260	0.262	0.262	0.262	0.261				
	V_p	X		3.458	7.331	7.585	7.754	7.870	7.951	8.116	8.179	8.205	8.222	8.236	8.167	1.02	1.00
				3.465	6.934	7.307	7.559	7.733	7.855	8.105	8.195	8.228	8.251	8.269	8.118	1.48	1.00
		Z		3.503	6.949	7.304	7.538	7.699	7.812	8.051	8.158	8.205	8.238	8.264	8.159	0.78	1.00
				3.475	7.071	7.399	7.617	7.767	7.873	8.091	8.177	8.213	8.237	8.256	8.148	1.09	
		A			5.402	3.798	2.836	2.202	1.766	0.803	0.257	0.000	0.194	0.339			
				3.458	4.319	4.408	4.468	4.509	4.539	4.607	4.643	4.659	4.671	4.680	4.752	0.55	1.00
		Y		3.465	4.359	4.480	4.559	4.614	4.651	4.731	4.768	4.785	4.797	4.807	4.650	0.80	0.99
				3.503	4.153	4.306	4.405	4.473	4.520	4.620	4.672	4.697	4.715	4.729	4.628	0.52	0.99
		$Mean$		3.475	4.277	4.398	4.477	4.532	4.570	4.653	4.694	4.714	4.728	4.739	4.677	0.62	
					0.935	1.637	2.032	2.317	2.451	2.665	2.663	2.673	2.665	2.680			
YT963	V_p/V_s	σ		1.653	1.682	1.701	1.714	1.723	1.739	1.742	1.742	1.742	1.742				
				0.212	0.227	0.236	0.242	0.246	0.253	0.254	0.254	0.254	0.254				
	V_p	X		3.436	7.321	7.449	7.554	7.641	7.714	7.932	8.061	8.086	8.092	8.095	8.072	0.24	0.96
				3.415	7.314	7.416	7.480	7.526	7.562	7.671	7.771	7.827	7.867	7.897	7.723	1.75	0.99
		Z		3.341	6.338	6.512	6.635	6.731	6.809	7.041	7.207	7.271	7.311	7.341	7.169	1.74	0.99
				3.397	6.991	7.126	7.223	7.299	7.361	7.548	7.680	7.728	7.757	7.778	7.655	1.24	
		A			14.060	13.149	12.718	12.462	12.289	11.806	11.120	10.537	10.071	9.698			
				3.436	4.416	4.442	4.459	4.472	4.483	4.520	4.553	4.567	4.576	4.583	4.545	0.38	0.99
		Y		3.415	4.202	4.242	4.272	4.298	4.319	4.391	4.449	4.469	4.478	4.484	4.448	0.36	0.98
				3.341	3.790	3.868	3.921	3.960	3.990	4.069	4.122	4.147	4.164	4.178	4.102	0.77	0.99
		$Mean$		3.397	4.136	4.184	4.218	4.243	4.264	4.327	4.375	4.395	4.406	4.415	4.365		

Table 3. (Continued).

Samples	V_p, V_s	λ^a	Density (g cm ⁻³)	V_p and V_s (km s ⁻¹) at Pressures (MPa)									$V_p(V_s) = V_0(V_{p0}/V_{s0}) + DP$			
				20	40	60	80	100	200	400	600	800	1000	V_0 (km s ⁻¹)	$D(10^{-4}$ km s ⁻¹ MPa ⁻¹)	R^2
UHP kyanite LJ01-1	V_p/V_s σ			1.690	1.703	1.713	1.720	1.726	1.745	1.755	1.759	1.760	1.762			
				0.231	0.237	0.241	0.245	0.247	0.255	0.260	0.261	0.262	0.262			
	V_p	X	3.582	8.385	8.563	8.693	8.795	8.878	9.235	9.293	9.351	9.386	9.412	9.263	1.50	0.99
		Y	3.580	7.857	8.123	8.325	8.485	8.615	8.993	9.219	9.282	9.315	9.339	9.198	1.43	0.99
		Z	3.582	8.181	8.421	8.588	8.714	8.811	9.068	9.221	9.284	9.326	9.359	9.173	1.88	0.99
		Mean	3.581	8.141	8.369	8.535	8.665	8.768	9.099	9.244	9.306	9.342	9.370	9.211	1.60	
	V_s	X	3.582	5.027	5.119	5.189	5.244	5.272	5.406	5.465	5.480	5.487	5.492	5.461	0.32	0.99
		Y	3.580	4.784	4.898	4.985	5.053	5.109	5.269	5.364	5.392	5.407	5.417	5.354	0.64	0.99
		Z	3.582	4.798	4.969	5.072	5.137	5.180	5.269	5.327	5.359	5.382	5.400	5.299	1.02	0.99
		Mean	3.581	4.869	4.995	5.082	5.144	5.192	5.314	5.386	5.410	5.425	5.437	5.371	0.66	
V_p/V_s σ				1.672	1.675	1.680	1.684	1.689	1.712	1.716	1.720	1.722	1.723			
				0.221	0.223	0.225	0.228	0.230	0.241	0.243	0.245	0.246				
UHP orthopyroxene MW01-3	V_p V_s		3.294	6.640	6.819	6.909	6.962	6.998	7.094	7.188	7.244	7.283	7.314	7.139	1.76	0.99
			3.294	3.917	3.957	3.985	4.005	4.021	4.068	4.104	4.120	4.130	4.138	4.092	0.47	0.99
	V_p/V_s σ			1.695	1.723	1.734	1.738	1.740	1.744	1.752	1.758	1.763	1.767			
				0.233	0.246	0.251	0.253	0.254	0.255	0.258	0.261	0.263	0.265			
	V_p	X	3.198	7.343	7.471	7.580	7.595	7.624	7.672	7.689	7.704	7.708	7.682	0.27	0.99	
		Y	3.261	7.289	7.437	7.513	7.555	7.580	7.625	7.657	7.675	7.688	7.699	7.641	0.58	0.99
		Z	3.205	6.961	6.999	7.027	7.050	7.069	7.127	7.170	7.185	7.192	7.197	7.166	0.32	0.99
		Mean	3.221	7.198	7.303	7.374	7.400	7.424	7.475	7.505	7.519	7.528	7.535	7.496	0.39	
	V_s	X	3.198	4.115	4.155	4.181	4.201	4.218	4.273	4.324	4.348	4.362	4.373	4.311	0.62	0.99
		Y	3.261	4.120	4.212	4.261	4.289	4.307	4.342	4.369	4.385	4.396	4.405	4.356	0.49	0.99
Z		3.205	3.795	3.887	3.940	3.972	3.992	4.028	4.048	4.060	4.068	4.074	4.039	0.36	0.99	
Mean		3.221	4.010	4.085	4.127	4.154	4.172	4.214	4.247	4.264	4.275	4.284	4.235	0.49		
V_p/V_s σ			1.795	1.788	1.787	1.781	1.779	1.774	1.767	1.763	1.761	1.759				
			0.275	0.272	0.272	0.270	0.269	0.267	0.264	0.263	0.262	0.261				
HP eclogite BX01-2	V_p	X	3.182	6.607	6.719	6.798	6.861	6.911	7.056	7.152	7.186	7.207	7.223	7.132	0.92	0.99
		Y	3.131	6.463	6.600	6.696	6.770	6.827	6.990	7.096	7.138	7.166	7.188	7.065	1.24	0.99
		Z	3.211	6.480	6.598	6.681	6.745	6.796	6.936	7.023	7.056	7.077	7.093	7.001	0.93	0.99
		Mean	3.175	6.517	6.639	6.725	6.792	6.845	6.994	7.090	7.127	7.150	7.168	7.066	1.03	
	V_s	X	3.182	3.782	3.912	3.990	4.039	4.071	4.135	4.170	4.190	4.203	4.214	4.153	0.62	1.00
		Y	3.131	3.838	3.908	3.957	3.994	4.022	4.093	4.130	4.143	4.153	4.160	4.119	0.41	0.99
		Z	3.211	3.879	3.979	4.037	4.074	4.098	4.149	4.185	4.206	4.221	4.233	4.167	0.66	0.99
		Mean	3.175	3.833	3.933	3.995	4.036	4.064	4.125	4.162	4.180	4.192	4.202	4.146	0.56	
	V_p/V_s σ			1.700	1.688	1.683	1.683	1.684	1.695	1.704	1.705	1.705	1.706			
				0.236	0.230	0.227	0.227	0.228	0.233	0.237	0.238	0.238	0.238			
CD962	V_p	X	3.341	7.464	7.590	7.672	7.729	7.770	7.865	7.921	7.949	7.969	7.984	7.897	0.88	0.99
		Y	3.288	6.835	6.988	7.094	7.175	7.239	7.416	7.530	7.576	7.607	7.630	7.496	1.35	0.99
		Z	3.202	6.845	6.992	7.089	7.158	7.210	7.346	7.438	7.485	7.518	7.544	7.398	1.48	0.99
		Mean	3.277	7.048	7.190	7.285	7.354	7.406	7.542	7.630	7.670	7.698	7.720	7.597	1.24	
	V_s	X	3.341	4.199	4.310	4.363	4.391	4.407	4.441	4.470	4.487	4.499	4.508	4.456	0.52	0.99
		Y	3.288	4.007	4.095	4.152	4.193	4.222	4.290	4.330	4.349	4.363	4.374	4.313	0.61	0.99
		Z	3.202	4.106	4.187	4.240	4.277	4.303	4.359	4.386	4.398	4.406	4.413	4.376	0.37	0.99
		Mean	3.277	4.104	4.197	4.252	4.287	4.311	4.363	4.395	4.411	4.423	4.431	4.382	0.50	
	V_p/V_s σ			1.717	1.713	1.713	1.715	1.718	1.728	1.736	1.739	1.741	1.742			
				0.244	0.242	0.242	0.243	0.244	0.248	0.252	0.253	0.254	0.254			
GQ961	V_p	X	3.469	6.897	7.150	7.305	7.408	7.479	7.646	7.766	7.834	7.882	7.919	7.708	2.12	0.99
		Y	3.457	6.235	6.647	6.915	7.098	7.227	7.508	7.659	7.734	7.788	7.830	7.752	2.40	0.99
		Z	3.432	6.550	6.710	6.825	6.914	6.985	7.191	7.326	7.376	7.407	7.430	7.296	1.35	0.99
		Mean	3.453	6.561	6.836	7.015	7.140	7.230	7.448	7.584	7.648	7.692	7.726	7.585	1.96	
	V_s	X	3.469	4.100	4.192	4.250	4.291	4.321	4.396	4.450	4.479	4.500	4.516	4.423	0.92	0.99
		Y	3.457	3.890	4.047	4.150	4.220	4.271	4.384	4.446	4.477	4.500	4.517	4.418	0.10	0.99
		Z	3.432	3.853	3.955	4.020	4.064	4.095	4.163	4.203	4.224	4.239	4.251	4.184	0.67	1.00
		Mean	3.453	3.948	4.065	4.140	4.192	4.229	4.314	4.366	4.393	4.413	4.428	4.342	0.56	
	V_p/V_s σ			1.662	1.682	1.694	1.703	1.710	1.726	1.737	1.741	1.743	1.745			
				0.216	0.227	0.233	0.237	0.240	0.248	0.252	0.254	0.255	0.255			
HZ964	V_p	X	3.254	6.595	6.787	6.907	6.989	7.047	7.189	7.293	7.351	7.393	7.425	7.242	1.85	0.99
		Y	3.216	6.646	6.814	6.924	7.002	7.060	7.205	7.301	7.351	7.386	7.413	7.258	1.56	0.99
		Z	3.182	6.673	6.802	6.894	6.965	7.020	7.178	7.280	7.318	7.343	7.362	7.254	1.09	0.99
		Mean	3.217	6.638	6.801	6.908	6.985	7.042	7.191	7.291	7.340	7.374	7.400	7.251	1.50	

Table 3. (Continued).

Samples	V_p, V_s	λ^a	Density (g cm ⁻³)	V_p and V_s (km s ⁻¹) at Pressures (MPa)									$V_p (V_s) = V_0(V_{p0}/V_{s0}) + DP$				
				20	40	60	80	100	200	400	600	800	1000	V_0 (km s ⁻¹)	$D(10^{-4}$ km s ⁻¹ MPa ⁻¹)	R^2	
HZ967	V_s	A	0.405	0.174	0.432	0.536	0.557	0.365	0.294	0.441	0.581	0.693					
		Y	3.254	3.867	3.922	3.958	3.985	4.007	4.074	4.130	4.157	4.176	4.190	4.109	0.82	0.99	
		Z	3.216	3.881	3.945	3.991	4.026	4.053	4.124	4.162	4.174	4.182	4.188	4.154	0.35	0.99	
		Mean	3.182	3.879	3.936	3.970	3.994	4.012	4.071	4.131	4.166	4.191	4.211	4.099	1.13	0.99	
		σ	3.217	3.876	3.934	3.973	4.001	4.024	4.090	4.141	4.166	4.183	4.196	4.121	0.77		
	V_p/V_s	A		0.045	0.217	0.526	0.800	1.004	1.300	0.747	0.199	0.219	0.545				
		σ		1.713	1.729	1.739	1.746	1.750	1.758	1.761	1.762	1.763	1.763				
		V_p	Y	3.111	6.195	6.383	6.514	6.611	6.683	6.860	6.949	6.982	7.005	7.023	7.098	0.63	0.99
		Z	3.095	6.236	6.405	6.525	6.615	6.683	6.850	6.928	6.954	6.971	6.984	6.922	1.02	0.99	
		Mean	3.100	6.284	6.468	6.597	6.690	6.759	6.923	6.997	7.024	7.042	7.056	6.976	0.76	0.99	
	XD962	V_s	A		2.923	3.265	3.411	3.438	3.400	3.011	2.668	2.582	2.536	2.500			
			Y	3.111	3.623	3.709	3.769	3.812	3.847	3.926	3.929	3.976	3.985	3.991	4.015	0.82	0.99
			Z	3.095	3.633	3.743	3.809	3.852	3.881	3.942	3.980	4.001	4.017	4.029	3.953	0.39	0.99
			Mean	3.100	3.637	3.744	3.811	3.855	3.886	3.954	3.981	4.012	4.025	4.036	3.976	0.60	
σ				0.876	1.889	2.216	2.271	2.174	1.741	2.666	2.046	2.226	2.365				
V_p/V_s		A		1.728	1.728	1.731	1.736	1.739	1.751	1.757	1.751	1.749	1.748				
		σ		0.248	0.248	0.250	0.252	0.253	0.258	0.261	0.258	0.257	0.257				
		V_p	Y	3.433	7.065	7.320	7.479	7.587	7.663	7.838	7.955	8.019	8.065	8.101	7.898	2.05	1.00
		Z	3.468	6.850	7.115	7.286	7.402	7.485	7.670	7.780	7.837	7.878	7.909	7.731	1.80	0.99	
		Mean	3.433	6.646	6.913	7.054	7.139	7.194	7.332	7.478	7.532	7.586	7.628	7.390	2.40	0.99	
XD966		V_s	A		6.114	5.720	5.844	6.074	6.298	6.646	6.165	6.247	6.107	6.003			
			Y	3.433	4.252	4.315	4.359	4.392	4.416	4.475	4.505	4.516	4.523	4.529	4.497	0.38	1.00
			Z	3.468	4.119	4.216	4.284	4.330	4.362	4.424	4.435	4.436	4.436	4.436	4.436	0.00	1.00
			Mean	3.433	3.988	4.107	4.174	4.214	4.238	4.283	4.310	4.325	4.335	4.344	4.297	0.48	1.00
	σ			4.120	4.213	4.272	4.312	4.339	4.394	4.417	4.426	4.431	4.436	4.410	0.27		
	V_p/V_s	A		6.408	4.937	4.330	4.128	4.103	4.370	4.415	4.316	4.243	4.170				
		σ		1.664	1.689	1.702	1.711	1.717	1.733	1.752	1.762	1.770	1.776				
		V_p	Y	3.102	6.000	6.315	6.545	6.721	6.860	7.238	7.450	7.519	7.563	7.596	7.405	1.92	0.99
		Z	3.083	5.980	6.271	6.477	6.632	6.752	7.065	7.237	7.302	7.345	7.379	7.188	1.93	1.00	
		Mean	3.117	5.673	5.974	6.183	6.337	6.454	6.756	6.928	7.001	7.052	7.091	6.868	2.25	0.99	
	XH961	V_s	A		5.884	6.187	6.402	6.563	6.689	7.020	7.205	7.274	7.320	7.355	7.154		
			Y	3.102	3.658	3.798	3.900	3.977	4.037	4.191	4.270	4.296	4.313	4.326	4.614	0.48	0.99
			Z	3.083	4.059	4.175	4.263	4.332	4.388	4.540	4.621	4.642	4.653	4.661	4.252	0.75	0.99
			Mean	3.117	3.629	3.762	3.855	3.925	3.979	4.119	4.198	4.228	4.249	4.265	4.173	0.92	0.99
σ				3.782	3.912	4.006	4.078	4.135	4.283	4.363	4.389	4.405	4.417	4.346	0.72		
V_p/V_s		A		11.370	10.558	10.185	9.980	9.892	9.829	9.695	9.433	9.171	8.965				
		σ		1.556	1.582	1.598	1.609	1.618	1.639	1.651	1.657	1.662	1.665				
		V_p	Y	3.293	7.140	7.292	7.401	7.486	7.555	7.756	7.890	7.939	7.968	7.990	7.864	1.28	0.99
		Z	3.285	6.573	6.781	6.915	7.008	7.076	7.239	7.343	7.397	7.436	7.466	7.295	1.73	0.99	
		Mean	3.232	6.511	6.703	6.828	6.916	6.981	7.139	7.242	7.294	7.332	7.361	7.195	1.67	0.99	
ZJ01-1		V_s	A		6.741	6.925	7.048	7.137	7.204	7.378	7.492	7.543	7.579	7.606	7.451		
			Y	3.293	4.130	4.183	4.216	4.241	4.260	4.315	4.360	4.384	4.401	4.413	4.341	0.72	0.99
			Z	3.285	3.996	4.046	4.081	4.108	4.132	4.208	4.274	4.301	4.316	4.326	4.264	0.62	0.99
			Mean	3.232	3.878	3.940	3.983	4.015	4.041	4.113	4.162	4.183	4.196	4.207	4.147	0.60	1.00
	σ			4.001	4.056	4.093	4.121	4.144	4.212	4.265	4.289	4.304	4.315	4.251	0.65		
	V_p/V_s	A		6.298	5.991	5.692	5.484	5.284	4.796	4.642	4.686	4.763	4.774				
		σ		1.685	1.707	1.722	1.732	1.738	1.752	1.756	1.759	1.761	1.762				
		V_p	Y	3.294	6.741	6.999	7.164	7.276	7.354	7.528	7.631	7.684	7.723	7.752	7.710	0.93	0.99
		Z	3.328	6.824	7.047	7.202	7.313	7.394	7.579	7.658	7.687	7.707	7.723	7.584	1.70	0.99	
		Mean	3.273	6.880	7.092	7.242	7.353	7.437	7.640	7.733	7.765	7.786	7.802	7.635	1.88	0.99	
	Granulite HL963	V_s	A		6.815	7.046	7.203	7.314	7.395	7.582	7.674	7.712	7.739	7.759	7.643		
			Y	3.294	3.968	4.062	4.130	4.181	4.222	4.327	4.383	4.402	4.414	4.423	4.422	0.56	0.99
			Z	3.328	4.040	4.126	4.190	4.239	4.278	4.386	4.445	4.463	4.473	4.481	4.371	0.52	0.99
			Mean	3.273	4.002	4.102	4.173	4.227	4.269	4.378	4.435	4.455	4.467	4.477	4.436	0.45	0.99
σ				4.003	4.097	4.164	4.216	4.256	4.364	4.421	4.440	4.451	4.460	4.410	0.51		
V_p/V_s		A		1.809	1.573	1.443	1.372	1.335	1.343	1.398	1.372	1.336	1.306				
		σ		1.702	1.720	1.730	1.735	1.737	1.738	1.736	1.737	1.739	1.740				
		V_p	Y	2.858	5.101	5.425	5.643	5.797	5.910	6.171	6.311	6.376	6.422	6.458	6.255	2.05	1.00
		Z	2.843	5.133	5.415	5.604	5.738	5.836	6.066	6.192	6.251	6.292	6.324	6.143	1.83	1.00	
		Mean	2.844	4.942	5.242	5.449	5.600	5.713	5.992	6.143	6.208	6.252	6.287	6.091	1.98	1.00	
			2.848	5.059	5.361	5.565	5.712	5.820	6.076	6.215	6.278	6.322	6.356	6.163	1.95		

Table 3. (Continued).

Samples	V_p, V_s	Z^a	Density (g cm^{-3})	V_p and V_s (km s^{-1}) at Pressures (MPa)										$V_p(V_s) = V_0(V_{p0}/V_{s0}) + \text{DP}$				
				20	40	60	80	100	200	400	600	800	1000	V_0 (km s^{-1})	$D(10^{-4} \text{ km s}^{-1} \text{ MPa}^{-1})$	R^2		
HL968	V_s	A	3.143	3.414	3.486	3.449	3.385	2.946	2.703	2.676	2.689	2.690						
		X	2.858	2.877	3.061	3.180	3.260	3.315	3.427	3.479	3.503	3.520	3.534	3.457	0.78	1.00		
		Y	2.843	3.008	3.141	3.228	3.286	3.325	3.407	3.443	3.461	3.473	3.483	3.428	0.55	1.00		
		Z	2.844	2.917	3.056	3.145	3.213	3.260	3.364	3.419	3.445	3.464	3.478	3.396	0.83	0.99		
		Mean	2.848	2.934	3.086	3.184	3.253	3.300	3.399	3.447	3.470	3.486	3.498	3.427	0.72			
	V_p/V_s	A		1.363	0.162	1.099	1.445	1.667	1.853	1.741	1.672	1.607	1.601					
		σ		1.724	1.737	1.748	1.756	1.764	1.788	1.803	1.809	1.814	1.817					
		σ		0.247	0.252	0.257	0.260	0.263	0.272	0.278	0.280	0.282	0.283					
		V_p	X	3.098	6.312	6.464	6.552	6.607	6.643	6.725	6.788	6.825	6.851	6.871	6.846	1.20	0.99	
		Y	3.124	6.458	6.527	6.580	6.623	6.658	6.764	6.834	6.855	6.865	6.872	6.829	0.44	0.99		
	HL969	V_s	Z	3.124	6.220	6.371	6.476	6.555	6.616	6.779	6.877	6.917	6.944	6.965	6.756	1.16	0.99	
			Mean	3.115	6.330	6.454	6.536	6.595	6.639	6.756	6.833	6.866	6.887	6.903	6.810	0.93		
			A		1.457	1.450	1.166	0.790	0.415	0.792	1.298	1.345	1.355	1.360				
			X	3.098	3.656	3.685	3.702	3.715	3.725	3.758	3.792	3.812	3.826	3.833	3.783	0.42	0.99	
			Y	3.128	3.640	3.661	3.675	3.686	3.695	3.722	3.746	3.756	3.763	3.768	3.740	0.28	0.99	
V_p/V_s		Z	3.124	3.502	3.596	3.654	3.692	3.718	3.769	3.794	3.808	3.817	3.825	3.782	0.52	0.97		
		Mean	3.117	3.599	3.647	3.677	3.698	3.712	3.750	3.778	3.792	3.802	3.808	3.768	0.41			
		A		0.451	0.659	0.748	0.795	0.826	0.947	1.224	1.469	1.655	1.717					
		σ		1.759	1.770	1.777	1.783	1.788	1.802	1.809	1.811	1.811	1.813					
		σ		0.261	0.265	0.268	0.271	0.273	0.277	0.280	0.281	0.281	0.281					
Amphibolite QJ961		V_p	X	3.094	6.103	6.309	6.441	6.531	6.595	6.742	6.832	6.879	6.913	6.939	6.790	1.50	0.99	
			Y	3.116	6.187	6.318	6.408	6.475	6.527	6.668	6.757	6.795	6.821	6.841	6.727	1.15	0.99	
			Z	3.114	5.808	6.040	6.184	6.282	6.352	6.551	6.671	6.751	6.809	6.854	6.599	2.58	0.99	
			Mean	3.108	6.033	6.222	6.344	6.429	6.491	6.654	6.753	6.808	6.848	6.878	6.705	1.74		
			A		4.890	4.323	4.051	3.873	3.743	2.871	2.384	1.880	1.519	1.236				
	V_s	X	3.094	3.382	3.461	3.513	3.549	3.574	3.624	3.640	3.646	3.650	3.653	3.636	0.17	0.99		
		Y	3.116	3.488	3.537	3.568	3.590	3.605	3.641	3.665	3.678	3.687	3.694	3.654	0.40	0.99		
		Z	3.114	3.361	3.446	3.504	3.545	3.575	3.646	3.683	3.700	3.712	3.721	3.669	0.52	0.99		
		Mean	3.108	3.410	3.481	3.528	3.561	3.585	3.637	3.663	3.675	3.683	3.689	3.653	0.36			
		A		0.616	0.431	0.255	0.112	0.028	0.605	1.174	1.470	1.683	1.843					
	BX01-6	V_p/V_s	σ		1.769	1.787	1.798	1.805	1.811	1.829	1.844	1.853	1.859	1.864				
			σ		0.265	0.272	0.276	0.279	0.281	0.287	0.292	0.294	0.296	0.298				
			V_p	X	3.067	5.989	6.128	6.225	6.300	6.360	6.537	6.663	6.714	6.747	6.772	6.628	1.45	0.99
			Y	3.066	4.970	5.391	5.684	5.898	6.057	6.438	6.624	6.697	6.747	6.786	6.565	2.23	0.99	
			Z	3.087	4.652	5.146	5.488	5.737	5.920	6.352	6.563	6.649	6.710	6.757	6.489	2.70	0.99	
Serpentine LW965		V_p	Mean	3.073	5.204	5.555	5.799	5.978	6.112	6.442	6.617	6.687	6.735	6.772	6.561	2.13		
			A		25.693	17.678	12.709	9.417	7.199	2.872	1.511	0.972	0.549	0.222				
			X	3.067	3.456	3.537	3.594	3.636	3.670	3.760	3.815	3.837	3.852	3.863	3.799	0.65	0.99	
			Y	3.066	2.946	3.244	3.436	3.562	3.648	3.814	3.884	3.917	3.940	3.958	3.856	1.03	1.00	
			Z	3.087	2.919	3.185	3.372	3.505	3.602	3.812	3.887	3.910	3.925	3.937	3.870	0.67	0.99	
		V_p/V_s	Mean	3.073	3.107	3.322	3.467	3.568	3.640	3.795	3.862	3.888	3.906	3.919	3.842	0.78		
			A		17.284	10.596	6.403	3.672	1.868	1.370	1.864	1.878	1.869	1.888				
			σ		1.675	1.672	1.672	1.676	1.679	1.697	1.713	1.720	1.724	1.728				
			σ		0.223	0.222	0.222	0.223	0.225	0.234	0.242	0.245	0.247	0.248				
			V_p	X	3.006	6.268	6.426	6.541	6.630	6.701	6.909	7.046	7.095	7.125	7.147	7.296	0.98	0.99
	Serpentine LW965	V_p	Y	3.008	6.097	6.334	6.501	6.627	6.726	7.002	7.178	7.250	7.298	7.336	7.124	2.13	0.99	
			Z	3.008	6.443	6.619	6.750	6.854	6.937	7.174	7.313	7.354	7.376	7.393	7.018	1.31	0.99	
			Mean	3.007	6.269	6.460	6.597	6.704	6.788	7.028	7.179	7.233	7.266	7.292	7.146	1.47		
			A		2.792	2.980	3.180	3.348	3.479	3.772	3.722	3.579	3.463	3.373				
			V_s	X	3.006	3.671	3.745	3.798	3.839	3.871	3.962	4.019	4.040	4.053	4.063	4.050	0.81	0.99
V_p/V_s		Y	3.008	3.342	3.570	3.726	3.840	3.924	4.128	4.237	4.285	4.319	4.345	4.197	1.49	1.00		
		Z	3.008	3.706	3.785	3.839	3.881	3.913	4.006	4.071	4.098	4.116	4.130	4.006	0.57	0.99		
		Mean	3.007	3.573	3.700	3.788	3.853	3.903	4.032	4.109	4.141	4.162	4.179	4.084	0.96			
		A		9.220	4.734	1.893	0.030	1.353	4.107	5.309	5.926	6.388	6.754					
		σ		1.755	1.746	1.742	1.740	1.739	1.743	1.747	1.747	1.746	1.745					
Serpentine LW965		V_p/V_s	σ		0.259	0.256	0.254	0.253	0.253	0.255	0.256	0.256	0.256	0.255				
			V_p	X	2.666	5.820	5.850	5.872	5.890	5.905	5.964	6.040	6.086	6.116	6.137	6.011	1.28	0.99
			Y	2.588	5.702	5.735	5.757	5.774	5.789	5.845	5.919	5.970	6.008	6.037	5.871	1.67	0.99	
			Z	2.600	5.687	5.716	5.736	5.752	5.765	5.816	5.885	5.934	5.971	6.000	5.836	1.67	1.00	
			Mean	2.618	5.736	5.767	5.788	5.805	5.820	5.875	5.948	5.997	6.032	6.058	5.906	1.54		
	V_s	A		2.319	2.324	2.350	2.377	2.406	2.519	2.606	2.535	2.404	2.261					
		X	2.666	2.897	2.903	2.906	2.909	2.911	2.921	2.931	2.937	2.942	2.946	2.923	0.23	1.00		
		Y	2.588	2.867	2.876	2.883	2.887	2.891	2.902	2.911	2.916	2.920	2.922	2.903	0.15	0.96		
		Z	2.600	2.967	2.993	3.009	3.019	3.025	3.040	3.051	3.058	3.062	3.066	3.046	0.20	1.00		
		Mean	2.618	2.910	2.924	2.933	2.938	2.942	2.954	2.964	2.970	2.975	2.978	2.957	0.19			
	V_p/V_s	A		3.436	4.001	4.296	4.492	4.554	4.671	4.723	4.781	4.774	4.835					
		σ		1.971	1.972	1.974	1.976	1.978	1.989	2.007	2.019	2.028	2.034					
		σ		0.327	0.327	0.327	0.328	0.328	0.331	0.335	0.337	0.339	0.341					

Table 3. (Continued).

Samples	V_p, V_s	λ^a	Density (g cm ⁻³)	V_p and V_s (km s ⁻¹) at Pressures (MPa)									$V_p (V_s) = V_0(V_{p0}/V_{s0}) + DP$			
				20	40	60	80	100	200	400	600	800	1000	V_0 (km s ⁻¹)	$D(10^{-4}$ km s ⁻¹ MPa ⁻¹)	R^2
Garnet-bearing phengite schist																
MY01-3	V_p	X	2.959	5.792	5.869	5.926	5.973	6.012	6.133	6.221	6.249	6.263	6.273	6.988	0.88	0.99
		Y	2.980	5.486	5.736	5.895	5.999	6.071	6.218	6.293	6.332	6.359	6.381	6.260	1.22	0.99
		Z	2.938	6.413	6.595	6.712	6.790	6.844	6.956	7.012	7.040	7.060	7.075	6.213	0.61	0.99
		Mean	2.959	5.897	6.067	6.178	6.254	6.309	6.436	6.509	6.540	6.561	6.577	6.487	0.90	
	V_s	A		10.540	11.980	12.717	13.065	13.189	12.786	12.162	12.097	12.141	12.195			
		X	2.959	3.409	3.542	3.622	3.671	3.704	3.768	3.806	3.827	3.842	3.853	3.971	0.78	0.99
		Y	2.980	3.477	3.593	3.664	3.710	3.740	3.798	3.825	3.839	3.849	3.857	3.813	0.45	0.99
		Z	2.938	3.625	3.742	3.812	3.856	3.886	3.949	3.993	4.017	4.035	4.048	3.787	0.67	0.99
	Mean	A	2.959	3.504	3.626	3.699	3.746	3.777	3.838	3.874	3.894	3.908	3.919	3.857	0.63	
		X		6.152	5.509	5.145	4.941	4.830	4.739	4.831	4.893	4.937	4.972			
		Y		1.683	1.673	1.670	1.670	1.671	1.677	1.680	1.679	1.679	1.678			
		Z		0.227	0.222	0.220	0.220	0.221	0.224	0.226	0.225	0.225	0.225			
Jadeite quartzite																
SH966	V_p	X	2.787	5.266	5.504	5.680	5.817	5.926	6.233	6.412	6.468	6.502	6.527	6.574	1.26	0.99
		Y	2.830	4.645	5.019	5.293	5.508	5.680	6.166	6.463	6.564	6.626	6.673	6.403	2.72	0.99
		Z	2.822	5.504	5.723	5.888	6.018	6.122	6.420	6.596	6.648	6.677	6.698	6.381	1.47	0.99
		Mean	2.813	5.138	5.415	5.620	5.781	5.909	6.273	6.490	6.560	6.601	6.633	6.453	1.82	
	V_s	A		4.630	4.049	3.699	3.468	3.309	2.984	2.842	2.742	2.655	2.584			
		X	2.787	3.161	3.310	3.416	3.496	3.559	3.730	3.830	3.868	3.893	3.912	3.952	1.60	0.99
		Y	2.822	3.272	3.447	3.562	3.642	3.701	3.846	3.940	3.989	4.024	4.051	3.897	1.55	1.00
		Z	2.830	2.978	3.217	3.385	3.512	3.608	3.857	3.993	4.046	4.082	4.110	3.803	1.10	0.99
	Mean	A	2.813	3.137	3.325	3.454	3.550	3.623	3.811	3.921	3.968	3.999	4.024	3.884	1.42	
		X		5.835	2.808	0.882	0.430	1.354	3.345	4.162	4.494	4.734	4.923			
		Y		1.638	1.629	1.627	1.628	1.631	1.646	1.655	1.653	1.651	1.648			
		Z		0.203	0.198	0.196	0.197	0.199	0.208	0.213	0.212	0.210	0.209			
Marble																
LW961	V_p	X	2.652	6.331	6.363	6.387	6.441	6.420	6.461	6.484	6.490	6.494	6.496	6.820	0.46	0.99
		Y	2.652	6.298	6.411	6.460	6.484	6.496	6.518	6.536	6.547	6.554	6.560	6.527	0.33	1.00
		Z	2.647	6.539	6.672	6.732	6.762	6.777	6.808	6.833	6.847	6.858	6.866	6.482	0.15	0.99
		Mean	2.650	6.389	6.482	6.526	6.562	6.565	6.596	6.618	6.628	6.635	6.640	6.610	0.31	
	V_s	A		3.252	4.774	5.297	4.893	5.445	5.252	5.266	5.383	5.483	5.561			
		X	2.652	3.260	3.275	3.287	3.297	3.304	3.326	3.338	3.340	3.341	3.341	3.392	0.12	0.99
		Y	2.652	3.424	3.429	3.437	3.442	3.446	3.458	3.471	3.480	3.486	3.490	3.464	0.27	1.00
		Z	2.647	3.297	3.323	3.342	3.355	3.364	3.386	3.396	3.400	3.402	3.405	3.338	0.04	0.99
	Mean	A	2.650	3.327	3.343	3.355	3.364	3.371	3.390	3.402	3.406	3.410	3.412	3.398	0.14	
		X		1.093	1.440	1.627	1.727	1.775	1.756	1.706	1.756	1.810	1.855			
		Y		1.920	1.939	1.945	1.950	1.947	1.946	1.946	1.946	1.946	1.946			
		Z		0.314	0.319	0.320	0.322	0.321	0.321	0.320	0.321	0.321	0.321			

^a λ refer to the three perpendicular directions, X parallel to lineation, Y perpendicular to lineation and Z normal to foliation.

0.281–0.298 in granulite and 0.248–0.255 in amphibolite, and significantly high values for serpentinite (0.341) and marble (0.321). In the low-grade metamorphic rocks, σ ranges from 0.209 to 0.224 (Table 3). The σ value for garnet-bearing orthopyroxenite (0.265) is close to that of eclogite. We also note a good correlation between σ and bulk-rock SiO₂ (Fig. 8b), with the exception of SH966 (jadeite quartzite), LJ01-1 (kyanite) and XD966 (eclogite). This linear trend is more significant than metamorphic grade, suggesting that σ cannot be used to infer metamorphic grade without considering rock compositions.

DISCUSSION

V_p, V_s pressure dependence

Pressure derivatives dV_p/dP and dV_s/dP of different lithologies are plotted as a function of bulk-rock density in Fig. 4. The majority of the dV_p/dP and dV_s/dP obtained in this work is less than 2×10^{-4} km s⁻¹ MPa⁻¹, with averages of 1.415 and

0.627×10^{-4} km s⁻¹ MPa⁻¹, respectively. These are lower than average values under pressures up to 600 MPa ($dV_p/dP = 4.429 \times 10^{-4}$ km s⁻¹ MPa⁻¹, $dV_s/dP = 1.503 \times 10^{-4}$ km s⁻¹ MPa⁻¹, Kern *et al.*, 1999, 2002; Gao *et al.*, 2001) and up to 800 MPa (2.272 & 1.317×10^{-4} km s⁻¹ MPa⁻¹, respectively; Wang *et al.*, 2005a,b, 2009; Ji *et al.*, 2007, 2009). The higher pressure derivative values (two–four times higher than this work) will overestimate wave velocities of the same lithologies at mantle pressures. For example, 2×10^{-4} km s⁻¹ MPa⁻¹ of dV_p/dP will result in velocity overestimate by ~ 0.2 and 0.3 km s⁻¹ at 2 GPa and 3 GPa, respectively. From these derivative data under 600–1000 MPa, it is apparent that under high confining pressures lower derivatives were obtained. Hence, we need to re-examine the effect of pressure on seismic velocity under mantle pressures so as to reliably estimate seismic velocity of mantle minerals under mantle conditions with confidence.

The data of pressure and temperature derivatives of V_p, V_s and density of eclogite and other important mantle rocks/minerals are summarized in Table 4.

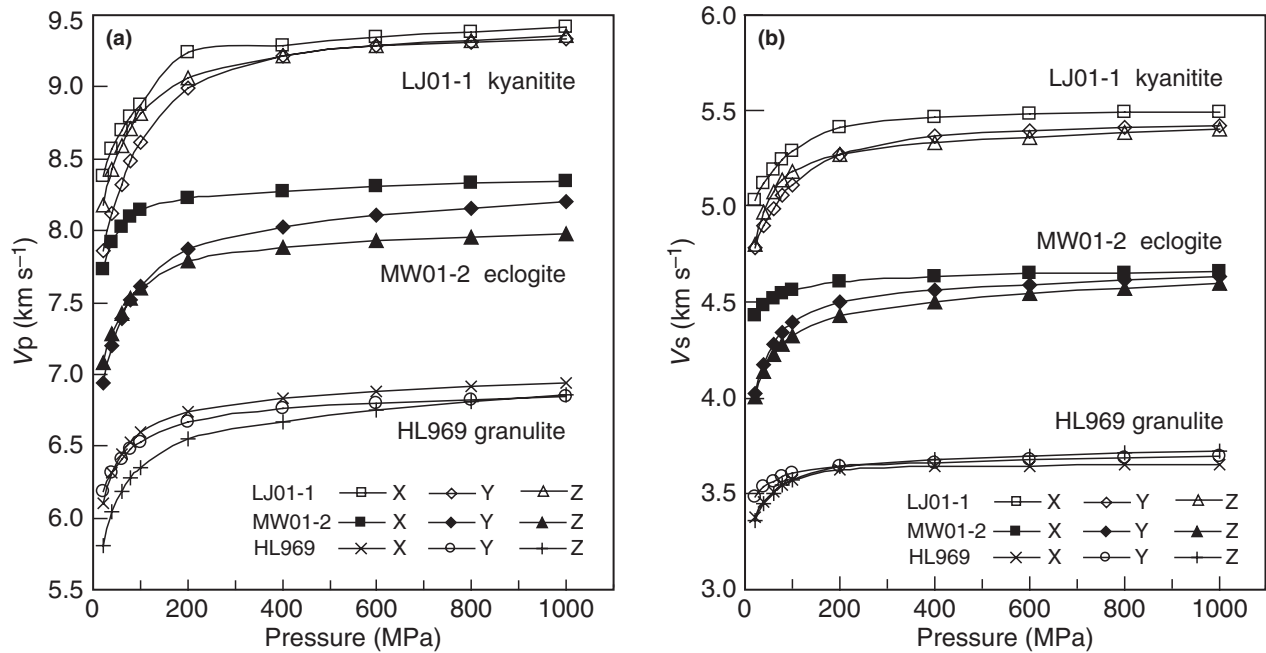


Fig. 3. V_p (a) and V_s (b) v. pressures (room temperature) of representative samples.

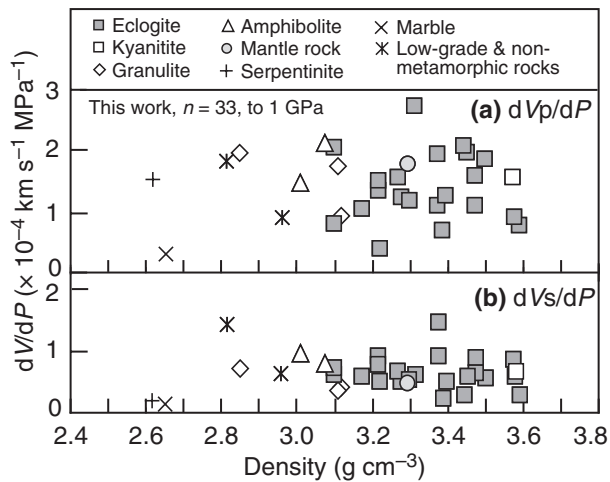


Fig. 4. Pressure derivatives dV_p/dP (a) and dV_s/dP (b) of the Dabie UHPM rocks plotted against density.

Olivine and its high-pressure polymorphs β -(Mg, Fe) $_2$ SiO $_4$ (wadsleyite) and γ -(Mg, Fe) $_2$ SiO $_4$ (perovskite, ringwoodite) are the most likely phases in the upper mantle, transition zone and lower mantle, where elastic properties of these minerals were documented at high pressures (up to 25 GPa) and high temperatures (see references in Table 4). The dV_p/dP and dV_s/dP (1.415 & $0.627 \times 10^{-4} \text{ km s}^{-1} \text{ MPa}^{-1}$, respectively) of eclogite in this work is the lowest among measured values under < 1 GPa pressure (Fig. 4), and is slightly higher than those for mantle rocks/minerals (0.4 – 1.1 & 0.1 – $0.3 \times 10^{-4} \text{ km s}^{-1} \text{ MPa}^{-1}$, respectively; Table 4). The

difference of $\sim 0.4 \times 10^{-4} \text{ km s}^{-1} \text{ MPa}^{-1}$ for dV_p/dP and $\sim 0.3 \times 10^{-4} \text{ km s}^{-1} \text{ MPa}^{-1}$ for dV_s/dP will lead to a significant overestimate of V_p by 0.4 km s^{-1} and of V_s by 0.3 km s^{-1} , respectively, at the mantle depth equivalent to 10 GPa.

The available temperature derivatives of V_p and V_s of eclogite (-3.4 to 2.1 & -1.0 to $0.4 \times 10^{-4} \text{ km s}^{-1} \text{ K}^{-1}$, respectively, Table 4) are consistent with the high-pressure mantle samples (-5 to -0.5 & -3.7 to $-0.4 \times 10^{-4} \text{ km s}^{-1} \text{ K}^{-1}$, respectively) at mantle depths. The only data of pressure derivatives of density ($d\rho/dP$, $0.395 \times 10^{-4} \text{ g cm}^{-3} \text{ MPa}^{-1}$) and temperature derivatives of density ($d\rho/dT$, $-0.678 \times 10^{-4} \text{ g cm}^{-3} \text{ K}^{-1}$) for eclogites obtained by Kern *et al.* (2002) are close to the mean values for mantle samples ($d\rho/dP = \sim 0.2 \times 10^{-4} \text{ g cm}^{-3} \text{ MPa}^{-1}$, $d\rho/dT = -1$ to $0.4 \times 10^{-4} \text{ g cm}^{-3} \text{ K}^{-1}$) under mantle conditions.

Overall, the pressure and temperature derivatives of V_p , V_s and density of eclogite are comparable to that of mantle-forming rocks/minerals at pressures up to 18 GPa (Table 4) (except for a slightly higher V_p and V_s), which allow us to extrapolate seismic velocity of eclogite to mantle depth (see below).

Elasticity of kyanite and its implications for crustal subduction

Kyanite is an important metamorphic index mineral for P – T conditions, but the elasticity of kyanite-rich rocks is lacking. The kyanite (sample LJ01-1, consist 99.5% kyanite and 0.5% corundum, Table 1) shows very high density (3.581 g cm^{-3}) and wave velocity ($V_p = 9.37 \text{ km s}^{-1}$, $V_s = 5.437 \text{ km s}^{-1}$ at 1000 MPa;

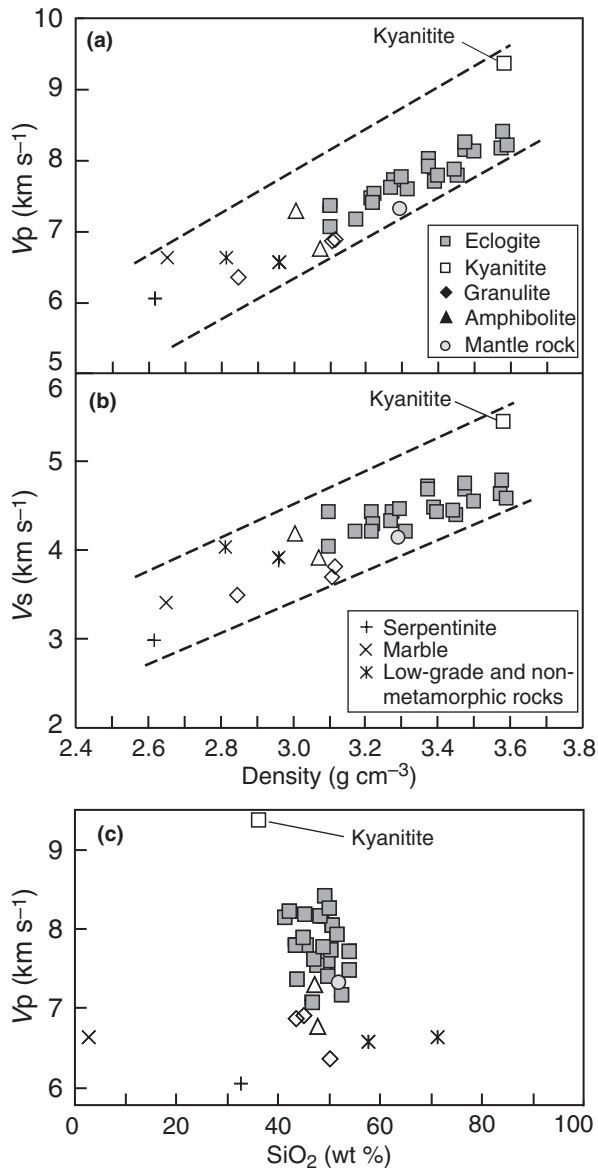


Fig. 5. Plots of mean V_p (a) and V_s (b) at 1000 MPa v. density, and V_p (1000 MPa) v. silica content (c).

Figs 3 & 5), which is comparable to rutile (9.43 & 5.43 km s^{-1}) and periclase (9.55 & 6.01 km s^{-1}), lower than spinel (10.08 & 5.86 km s^{-1}) and corundum (10.89 & 6.45 km s^{-1}), but significantly greater than garnet, one of the important major mantle minerals (8.52 & 4.77 km s^{-1}), and olivine (8.56 & 4.98 km s^{-1}) (Birch, 1961). These new data on kyanite suggest that the kyanite-rich rocks, whether transformed from recycled oceanic crustal gabbroic rocks or troctolite (Spetsius, 2004; Zhang *et al.*, 2008), or continent-derived sediments (Rapp *et al.*, 2008; Wang *et al.*, 2010), have the chance to achieve very high velocity and density significantly greater than the surrounding mantle rocks. Although kyanite, with ultra-high

density and velocity, is often found in granulite facies metamorphic rocks of pelitic protoliths, in some UHP metamorphic rocks, and even in kyanite deposits (Beane & Field, 2007; Dill, 2007), it does not contribute significantly to the bulk-rock density and velocity because of its low modal abundances in common rocks. However, its significance needs considering when the protoliths are Al_2O_3 rich rocks like pelite (metamorphosed to rocks of kyanite–jadeite–quartz/coesite assemblage) or troctolite (metamorphosed to kyanite-rich eclogite), in which case kyanite may become important, especially when this mineral may be locally concentrated as a result of metamorphic/deformational differentiation in subducting/subducted crustal materials under mantle conditions.

Since the kyanite has very low V_p -A and V_s -A (0.563 & 1.375% at 1 GPa, respectively, Table 3), it can be approximately treated as an isotropic material (Fischer-Cripps, 2000), and the elasticity data (bulk moduli K , shear moduli G , and elastic moduli E) can be approximated for the whole-rock samples using the following equations (Birch, 1961):

$$\rho = \rho_0 + 0.395P$$

$$K = \rho(V_p^2 - \frac{4}{3}V_s^2)$$

$$G = \rho V_s^2$$

$$E = 3K(1 - 2\sigma)$$

Where ambient density ρ_0 , V_p , V_s , and σ are from this experiment shown in Table 3, P is pressure (in GPa), 0.395×10^{-4} $\text{g cm}^{-3} \text{ MPa}^{-1}$ is the density derivative $d\rho/dP$ from the average value for UHPM rocks of Kern *et al.* (2002). The final results of K , G , E as well as their pressure derivatives by least-square solution from the linear portion of 0.4 to 1.0 GPa are shown in Table 5 and Fig. 9. The bulk moduli K of kyanite ranges from 124 to 180 GPa in the pressure range of 0.02–1.0 GPa, with $K_0 = 163$ GPa at zero pressure, which is close to 156 GPa (with $dK/dP = 5.6$) or 160 GPa (with dK/dP fixed at 4.0) by XRD methods (Comodi *et al.*, 1997), but lower than the values of single mineral kyanite, 193 GPa by compressibility studies (Yang *et al.*, 1997a,b), 192–201 GPa by synchrotron X-ray diffraction (Liu *et al.*, 2009), 178 GPa by a density functional theory and 223 GPa using a coreshell model (Winkler *et al.*, 2001). The bulk modulus for kyanite is similar to most common upper mantle minerals (see compilation of Niu & Batiza, 1991). The shear moduli G of our kyanite ranges from 85 to 110 GPa, with the ambient value of 102 GPa. The elastic moduli E ranges from 208 to 273 GPa (0.02–1.0 GPa), with the zero pressure E_0 value of 253 GPa (Fig. 9). The E values in this study are similar to values of 186–253 GPa obtained using

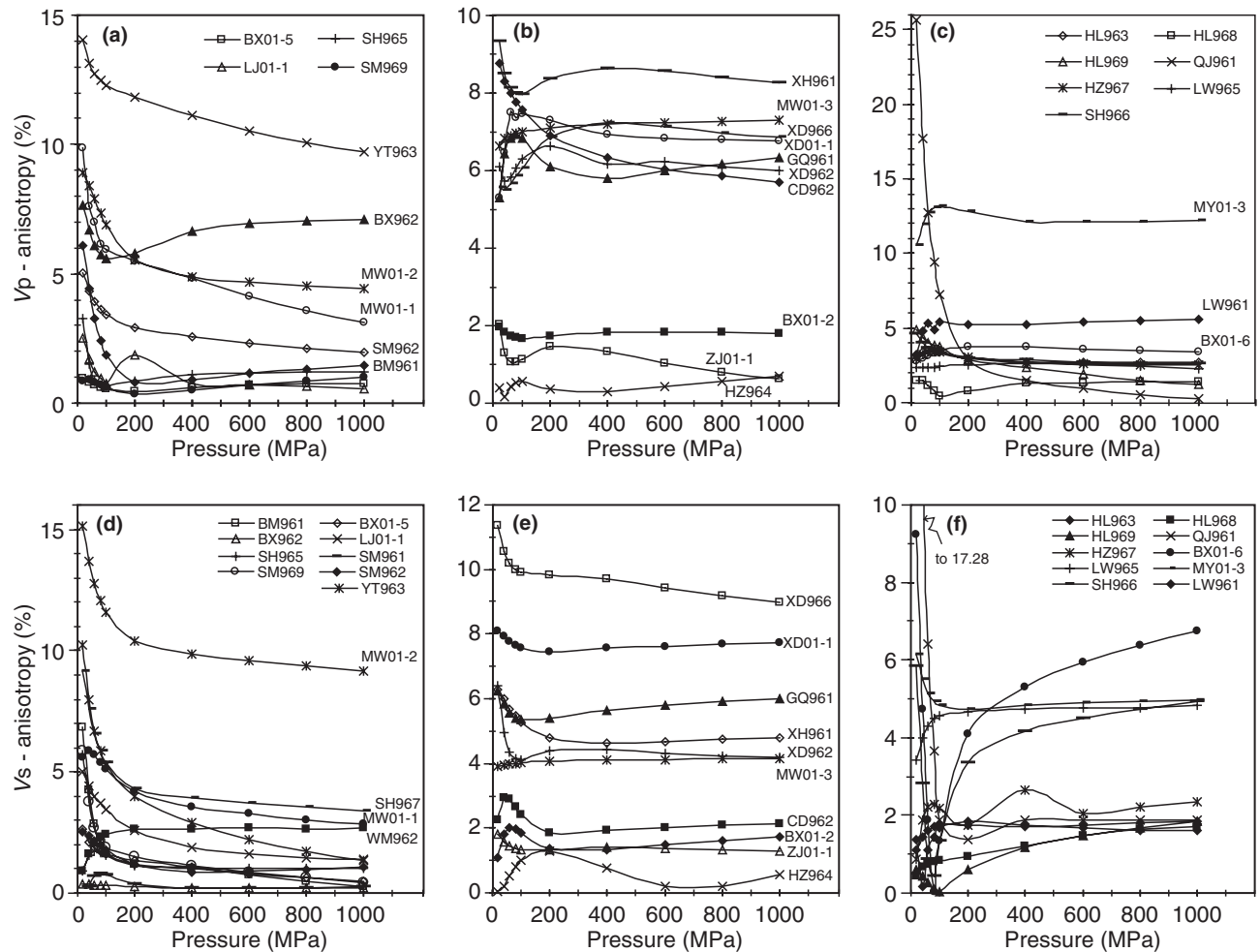


Fig. 6. Anisotropy of V_p (a, b, c) and V_s (d, e, f) variations with pressures.

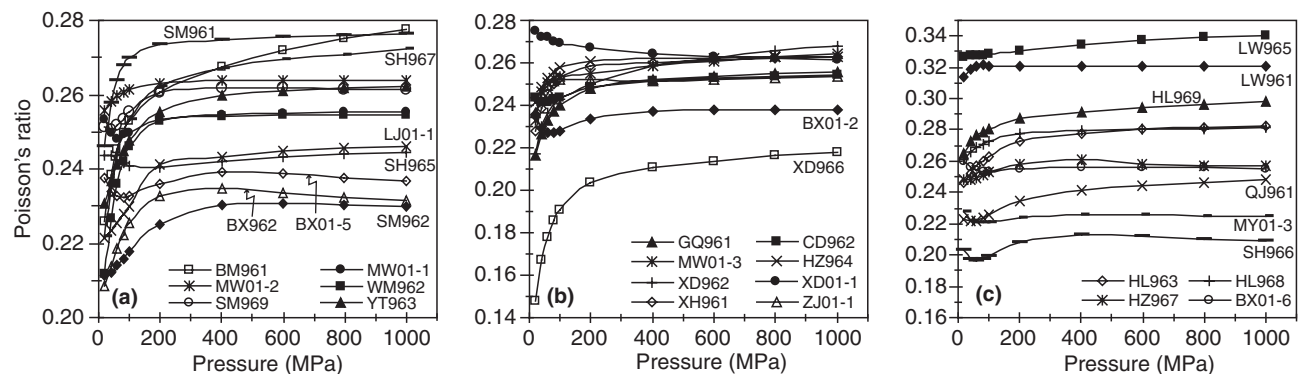


Fig. 7. Poisson ratio changing with pressures.

depth-sensing indentation for the three measured planes for an applied load of 100 mN (Whitney *et al.*, 2007), but lower than the calculated values 268–348 GPa (Comodi *et al.*, 1997; Yang *et al.*, 1997a,b; Winkler *et al.*, 2001; Mikowski *et al.*, 2008) and

297 ± 11 GPa of the perfect cleavage (100) and 405 ± 31 GPa of plane (010) (Mikowski *et al.*, 2008). Our results of the elasticity of kyanite (with nearly pure kyanite) are potentially useful and important for illustrating the nature, phase transformations, and for

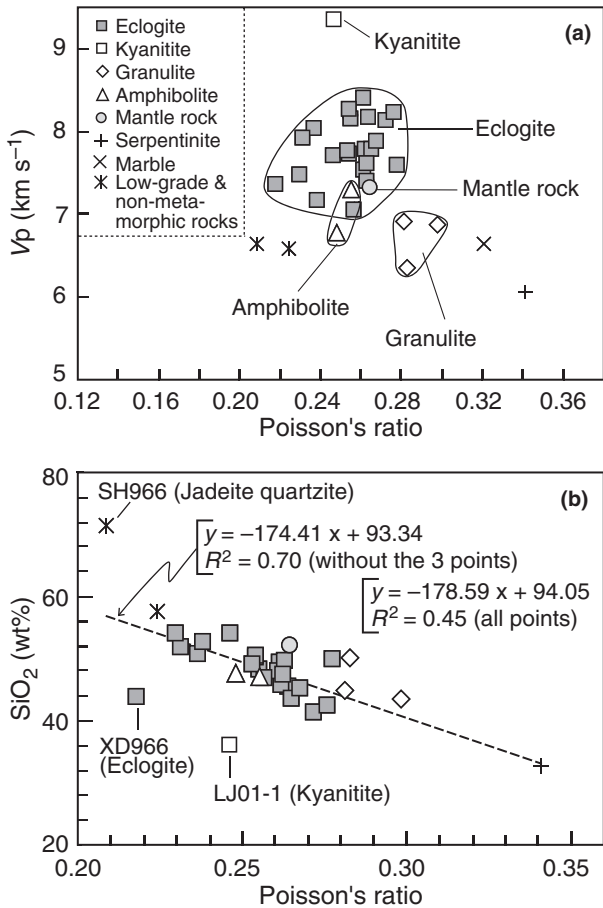


Fig. 8. Mean V_p at 1 GPa (a) and SiO_2 (b) plotted with Poisson's ratio in the Dabie rocks.

microstructural models of Al_2SiO_5 deformation behaviour, during subducting journey of crustal materials (i.e. terrigenous sediments) to mantle depths.

Serpentinization of olivine-bearing mantle rock

The significant decrease in V_p , V_s , and ρ and increase of σ take place during serpentinization. Though the major element compositions do not change, the seismic properties of serpentinite ($\rho = 2.618 \text{ g cm}^{-3}$; $V_p = 6.1 \text{ km s}^{-1}$, $V_s = 3.0 \text{ km s}^{-1}$, $\sigma = 0.341$ at 1 GPa, this work) differ markedly from dunite. Serpentinites have the lowest density and wave velocities (even lower than the common crustal low-grade metamorphic rocks) and very high σ (Figs 5 & 8). This serpentinization-induced physical property change of olivine have long been studied in the laboratories (Hess, 1959, 1962; Birch, 1961; Christensen, 1972, 1996, 2004), and also observed in seismic images on top of the subducting slabs (Peacock, 2001; Bostock *et al.*, 2002; Hyndman & Peacock, 2003; Kawakatsu & Watada, 2007). The presence of serpentines will facilitate many geodynamic processes under subduction-zone ultra-deep conditions. First, the hydrous serpentine minerals (especially the

Table 4. Compiled pressure and temperature derivatives of V_p , V_s and density of eclogites and mantle-forming rocks/minerals.

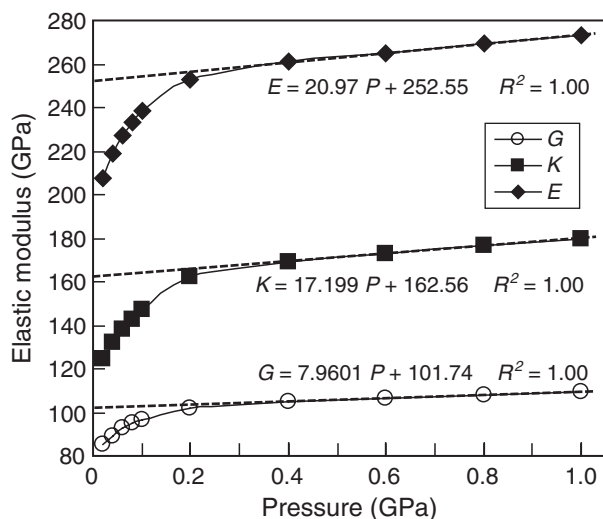
Rock/mineral (Nos)	P (GPa)/T(K)	$dV_p/dP(\times 10^{-4})$ $\text{km s}^{-1} \text{MPa}^{-1}$	$dV_s/dP(\times 10^{-4})$ $\text{km s}^{-1} \text{K}^{-1}$	$d\rho/dP(\times 10^{-4})$ $\text{g cm}^{-3} \text{MPa}^{-1}$	$dV_p/dT(\times 10^{-4})$ $\text{km s}^{-1} \text{K}^{-1}$	$d\rho/dT(\times 10^{-4})$ $\text{g cm}^{-3} \text{K}^{-1}$	References
Eclogite ($N = 22$)	1 GPa	1.415	0.627				This work
Eclogite ($N = 18$)	5 GPa/1573 K	2.2-3.3					[1, 2]
Dabie-Sulu eclogite	0.6 GPa/873 K	4.4 ($N = 24$)	-3.4				[3, 4, 5]
Dabie-Sulu eclogite	0.8 GPa	1.80 ($N = 40$)	-2.1 ($N = 24$)	0.395 ($N = 14$)	-1.0 ($N = 24$)	-0.678 ($N = 14$)	[6, 7]
Dabie-Sulu eclogite ($N = 42$)	0.8 GPa	2.276					[8]
Eclogite ($N = 2$)	3 GPa	0.97					[9]
Mantle-forming rocks/mineral							
Majorite garnet	18 GPa/1473 K	0.44-0.57					[11]
Majorite-pyroxene	700 km/1673 K						[11]
Forsterite-Fayalite (α)	1700 K						[11-15]
Polycrystalline olivine(α)	10.5 GPa/1773 K	~1.1					[16]
Polycrystalline olivine(α)	12.5 GPa/1673 K	~0.8					[17]
Olivine (α)	12 GPa	0.78					[18]
Wadsleyite, β -(Mg,Fe) $_2$ SiO $_4$	12 GPa	0.63					[18]
Ringwoodite, γ -(Mg $_{0.9}$ Fe $_{0.09}$) $_2$ SiO $_4$	18 GPa/1273 K	0.47-0.56					[19]
Wadsleyite-Ringwoodite	700 km/1673 K						[11]

References: [1] Zhao *et al.*, 1998; [2] Zhao *et al.*, 1999; [3] Kern *et al.*, 2002; [5] Cao *et al.*, 2001; [6] Wang *et al.*, 2005a; [7] Wang *et al.*, 2005b; [8] Ji *et al.*, 2007; [9] Christensen, 1974; [10] Irfune *et al.*, 2008; [11] Sinogeikin & Bass, 2002; [12] Suzuki *et al.*, 1983; [13] Isak *et al.*, 1989; [14] Sumino, 1979; [15] Graham *et al.*, 1988; [16] Knoche *et al.*, 1997; [17] Zang *et al.*, 1993; [18] Li *et al.*, 1996; [19] Higo *et al.*, 2008.

Table 5. Elasticity and density of kyanite at zero pressure and 0.02–1.0 GPa.

Pressure (GPa)	ρ (g cm ⁻³)	K (GPa)	G (GPa)	E (GPa)
Derivatives	$d\rho/dP = 0.395$ (10^{-4} g cm ⁻³ MPa ⁻¹) ^a	$dK/dP = 17.2$	$dG/dP = 8$	$dE/dP = 20.9$
0	$\rho_0 = 3.581$	$K_0 = 163$	$G_0 = 102$	$E_0 = 253$
0.02	3.582	124.2	84.9	207.5
0.04	3.584	131.8	89.4	218.8
0.06	3.586	137.8	92.6	227.0
0.08	3.589	142.8	95.0	233.3
0.1	3.593	147.1	96.9	238.3
0.2	3.601	162.5	101.7	252.5
0.4	3.617	169.2	104.9	260.8
0.6	3.641	173.2	106.6	265.3
0.8	3.672	176.4	108.1	269.3
1.0	3.712	179.6	109.7	273.4

^a $d\rho/dP = 0.395 \times 10^{-4}$ g cm⁻³ MPa⁻¹ is the average of 14 eclogites from Kern *et al.* (2002).

**Fig. 9.** Calculated bulk moduli K , shear moduli G , and elastic moduli E v. pressures in kyanite rock.

high P - T polymorph antigorite) are among the major agents that store and transport water to the mantle (Hyndman & Peacock, 2003). The incomplete subduction-zone dehydration (Niu, 2004) can effectively carry into deep mantle much water along with water-soluble elements (e.g. Ba, Rb, Cs, U, K, Sr), contributing to mantle compositional heterogeneity, and probably the HIMU (i.e. high U/Pb) component in mantle source regions of some oceanic basalts (Niu, 2004). Second, it can weaken the plate boundary/rock interfaces, assisting slip and subduction (Hilaret *et al.*, 2007), and other processes such as buoyancy-facilitated exhumation of UHPM eclogites. Third, if serpentines experience dehydration reaction from antigorite to forsterite + enstatite + H₂O, which can be imaged seismically, earthquakes may occur as a result by means of dehydration embrittlement within subducting slabs (Peacock, 2001; Dobson *et al.*, 2002; Hacker *et al.*, 2003).

Density and velocity constraints on lithosphere delamination and ultra-deep subduction

The density difference between the subducted eclogites with the underlying lower continental crust and its neighbouring mantle rocks at upper mantle conditions has been regarded as the essential cause for delamination (Gao *et al.*, 2004; Anderson, 2005). Here, two typical UHPM rocks (eclogite SM969 & kyanite LJ01-1) with the highest wave velocity and density were selected for density and wave velocity extrapolation to 15 GPa following a reasonable geotherm (Akaogi & Ito, 1993; Jephcoat, 1998). The following equations are used for V_p and density calculations applicable to upper mantle depths as a function of pressure and temperature:

$$V_p = V_{p0} + (dV_p/dP)P + (dV_p/dT)T$$

$$\rho = \rho_0(d\rho/dP)P + (d\rho/dT)T$$

Where V_{p0} and ρ_0 are V_p and ρ at zero pressure, respectively. The pressure derivatives dV_p/dP are from this work, the temperature derivatives ($dV_p/dT = -2 \times 10^{-4}$ km s⁻¹ K⁻¹) are from Kern *et al.* (1999, 2002). For density calculation, the average pressure coefficient ($d\rho/dP = 0.495 \times 10^{-4}$ g cm⁻³ MPa⁻¹) and temperature coefficient ($d\rho/dT = -0.678 \times 10^{-4}$ g cm⁻³ K⁻¹) from Kern *et al.* (2002) are used.

The final density and V_p results for our samples at mantle depths are plotted with the standard one-dimensional global seismic model for comparison (Fig. 10). The V_p values of UHPM rocks are equal to or greater than that of the ambient mantle, yielding the maximum contrast of $\Delta V_p > 0.3$ km s⁻¹. This suggests that subducted UHPM rocks will have higher velocity than the ambience in the upper mantle, as recognized seismically. By assuming no phase changes involved, the density contrast between UHPM rocks and the ambient mantle is $\Delta\rho > 0.3$ – 0.4 g cm⁻³. The significant density differences (> 0.3 – 0.4 g cm⁻³) of subducted UHPM rocks, including eclogite and kyanite in this work, meta-greywacke and meta-pelite of crustal-affinity (Massonne *et al.*, 2007) and jadeite stishovite-bearing rocks (Wu *et al.*, 2009; Wang *et al.*, 2010), with respect to the ambient upper mantle, are greater than previously predicted, and support the density-contrast controlled delamination models (Bird, 1978, 1979; Arndt & Goldstein, 1989; Kay & Kay, 1991; Gao *et al.*, 2004, 2008; Anderson, 2005). Here, we refer delamination to a large scale detachment of down-going oceanic/continental slabs, or the lower parts of thickened orogenic lithosphere, from the upper parts of the slabs/lithosphere.

In addition to density contrast, other factors have also been taken into account in recent delamination models. Deformation experiments show that garnet is strong in crustal depths (< 850 °C), but shows thermal

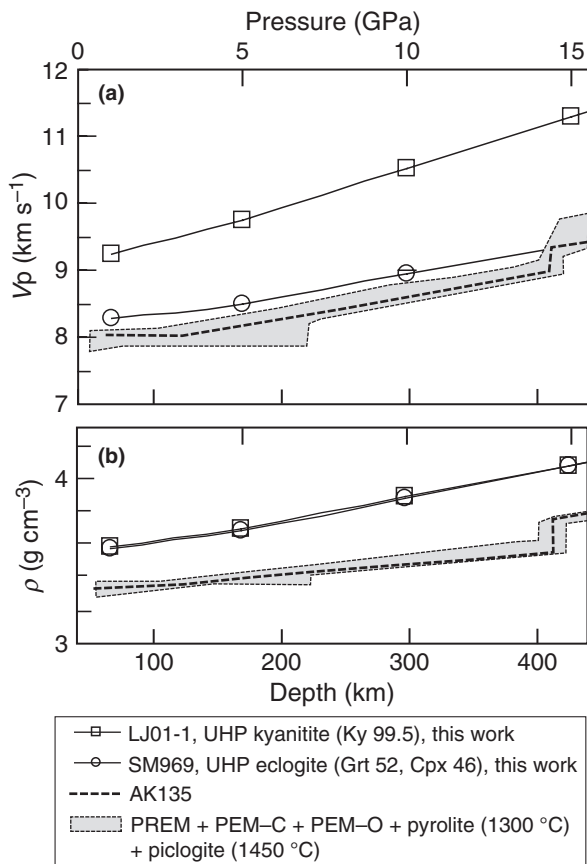


Fig. 10. Extrapolated V_p (a), and density ρ (b) in two representative UHPM rocks to upper mantle depth with simultaneous pressure and temperature. The one-dimensional global seismic models (AK135, PREM, PEM-O, and PEM-C) and calculated pyrolitic mantle following a 1300 °C adiabat and piclogitic mantle following a 1450 °C adiabat are all from Cammarano *et al.* (2003).

weakening at high temperatures (Ji *et al.*, 1998; Wang & Ji, 1999). The rheology experiment of eclogite at 3 GPa (Jin *et al.*, 2001) shows that flow properties of eclogites are the same as peridotite, which suggest that delamination of oceanic crust from the underlying mantle lithosphere due to rheological contrast is unlikely during subduction either at shallow mantle depths or in the lower part of the mantle transition zone (500–700 km). Moore & Wiltshko (2004) emphasized that syncollisional delamination most likely occurs in response to negative buoyancy. Eclogite (SM 969) and especially kyanite with ‘extreme’ velocity and density are rare lithologies. However, under the conditions of thickened crust, their local abundances in the deep crust can certainly contribute to such negative buoyancy, thus facilitating delamination. Although cases of delamination have been well documented, how delamination actually initiates remains under debate (Doglioni *et al.*, 2007).

At least two ways can be used to identify a delaminated and ultra-deep subducted slab. One is direct

seismic observation, and the other is indirect inference using the geochemistry of mantle-derived magmas (Kay & Kay, 1991; Gao *et al.*, 2004, 2008; Liu *et al.*, 2008). High resolution seismic tomography has revealed many such materials beneath subduction zones, young and fossil orogens and rift systems globally (e.g. Zhao, 2004; Ren & Shen, 2008; Yang, 2009). For instance, seismic tomography beneath the Dabie–Sulu orogen revealed a slab-like high velocity anomaly from the Moho down to 110 km depth, and the high velocity materials most probably represent subducted Yangtze lithosphere as a result of its collision with the North China craton since the early Mesozoic (Xu *et al.*, 2001). Usually, the velocity difference of $\sim \pm 2\%$ for V_p between the foundering high velocity UHP assemblage and the ambient mantle can be distinguished using modern geophysical methods. In the Dabie–Sulu region, a V_p contrast up to 18% exists between the high velocity subducted slab and the adjacent low velocity mantle (Xu *et al.*, 2001). In our extrapolation (Fig. 10), 0.3 km s^{-1} V_p difference between UHPM eclogite and the mantle is $\sim > 4\%$. Thus, the UHP metamorphic rocks can be recognized as high velocity layer/slab by seismic tomography. Geochemically, mantle-derived magmas can be used to infer mantle lithosphere delamination. For example, the ~ 130 Ma post-collisional mafic-ultramafic intrusive rocks with typical ‘continental’ features from the North Dabie region is probably a magmatic response to the collision-related mantle lithosphere delamination (Li *et al.*, 1998a,b, 2002; Ma *et al.*, 1998; Jahn *et al.*, 1999; Fan *et al.*, 2004; Zhang *et al.*, 2004; Wang *et al.*, 2005c; Zhao *et al.*, 2005; Huang *et al.*, 2007).

Delamination can explain not only the recycling of crustal materials back to the mantle, but also the exhumation of UHPM rocks from depths in excess of ~ 80 km (> 2.5 GPa) (Fig. 11). The density contrast between UHP eclogites and the upper mantle (> 0.3 – 0.4 g cm^{-3}) will depress the dense eclogite, which will eventually detach from the subducted less dense continental crust of the upper slab and sink into the deeper mantle, if their density is higher than the critical buoyancy of the underlying mantle rocks. Thus, we envisage a ‘spring’ inside the subducted slab, which will break down when delamination occurs. The stagnant slabs possibly represent the delaminated materials with a high velocity anomaly. Meanwhile, the lower density jadeite- and coesite-bearing felsic gneisses in the upper part of the subducted slab remain less dense, and yield sufficient buoyancy to overcome frictional resistance, and thus separate from the delaminating eclogites. This concept is consistent with the observation that all the documented HP–UHP complexes consist dominantly ($> 90\%$) of low-density granitic gneisses of crustal protoliths (Ernst & Liou, 2008) with volumetrically minor eclogite and fragments of mantle peridotite (e.g. Song *et al.*, 2005) picked up during exhumation (Green *et al.*, 1997, 2000). This model, which combines ultra-deep subduction and UHPM rock exhumation

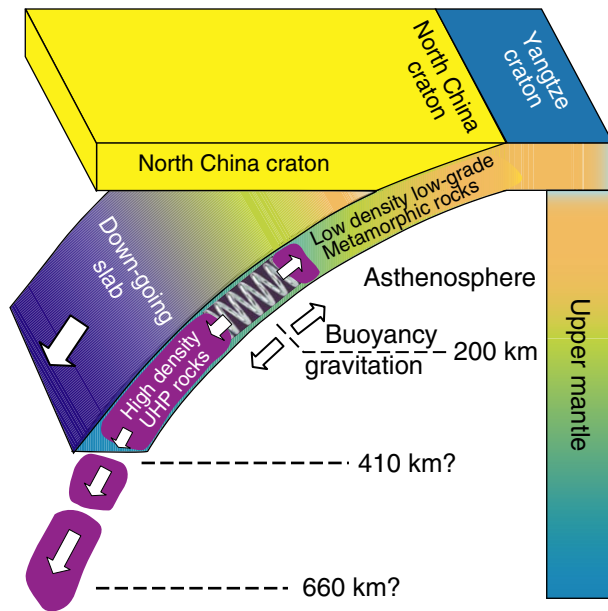


Fig. 11. Cartoon showing the UHPM rocks subducted in the down-going slab. If the delamination happened (the spring broke-down), the less dense upper part abundant in low grade crustal materials will return back to crustal level, leaving the dense lower part going down to depth.

together, is thus far the best explanation for the exposure of HP and UHP eclogites (Liou *et al.*, 1997). From the above, we propose that most of the eclogite founders into deeper mantle and only a small volume returns to crustal depths.

The above delamination concept can help explain lithosphere thinning and crustal foundering associated with subduction and continental collision. However, the actual physical processes of delamination remain to be further studied, and may not be the sole mechanism for lithosphere thinning. For example, the Mesozoic lithosphere thinning and related basaltic magmatism in eastern China can be explained by other processes without invoking delamination by Niu (2005).

CONCLUSIONS

We present measurements of the zero-pressure density and V_p and V_s data of 33 samples from the Dabie UHPM belts at pressures up to 1 GPa. The samples are mostly eclogites plus minor lithologies such as serpentinite, pyroxenite, granulite and kyanite. The major observations and conclusions are as follows:

1. V_p and V_s increase rapidly with increasing confining pressures from 0 to 0.3 GPa, and then increases linearly from 0.3 to 1 GPa. The majority of the dV_p/dP and dV_s/dP values in the bulk-rock samples are less than $2 \times 10^{-4} \text{ km s}^{-1} \text{ MPa}^{-1}$, with mean values of 1.415 and $0.627 \times 10^{-4} \text{ km s}^{-1} \text{ MPa}^{-1}$, respectively. At 1 GPa, the UHP eclogites have high V_p , V_s and densities, whereas the UHP orthopyroxenite, HP

eclogites, granulite and amphibolite are relatively low. The kyanite has very high wave velocity and density.

2. At 1 GPa, V_p - and V_s -A vary as much as 12%. The 22 UHP and HP eclogites yield more variable V_p -A (0.34–9.70%) and V_s -A (0.2–9.17%). The kyanite has very low anisotropy (0.56 & 1.38%, respectively). The Poisson's ratios along with V_p and SiO_2 show clear lithological and metamorphic grade dependence, ranging from 0.218 to 0.278 for HP and UHP eclogites, 0.281–0.298 for granulite and 0.248–0.255 for amphibolite. The higher values are found for serpentinite (0.341) and marble (0.321).
3. Based on measured data, the elasticity moduli K , G , E of kyanite were obtained. The bulk moduli K of kyanite is 180 GPa at 1 GPa, and $K_0 = 163$ GPa at zero pressure. The shear moduli G is 110 GPa at 1 GPa and 102 GPa at zero pressure. The elastic moduli E of kyanite is 273 GPa at 1 GPa and 253 GPa at zero pressure.
4. The V_p and density of two UHPM rocks were calculated to mantle depths up to ~ 15 GPa to trace the positive difference between UHPM rocks and the surrounding mantle ($\Delta V_p > 0.3 \text{ km s}^{-1}$, $\Delta \rho > 0.3\text{--}0.4 \text{ g cm}^{-3}$). These results are useful for understanding density-induced delamination processes that may take place during and soon after continental collision such as in the Sulu–Dabie orogenic belt in the early Mesozoic in eastern China.

ACKNOWLEDGEMENTS

This work was supported by the National Key Project for Basic Research (2009CB421002, 2011CB403102), SinoProbe-04-02 project, NSF of China (91014003, 40873023, 40830317, and 49672142), China Geological Survey, 111 project (B07011), to the authors in China; and a Leverhulme Research Fellowship, Durham University Christopherson/Knott Fellowship and Lecturer Professorship at China University of Geosciences, Beijing to Y. Niu. X. Liu and W. Zhu provided assistant during the field work. We thank H. Kern and an anonymous reviewer for constructive comments that have helped greatly improve this manuscript. D. Whitney and D. Robinson are thanked for their helpful comments and editorial handling.

REFERENCES

- Akaogi, M. & Ito, E., 1993. Heat capacity of MgSiO_3 perovskite. *Geophysical Research Letters*, **20**, 105–108.
- Anderson, D.L., 2005. Large igneous provinces, delamination, and fertile mantle. *Elements*, **1**, 271–275.
- Arndt, N.T. & Goldstein, S.L., 1989. An open boundary between lower continental crust and mantle: its role in crust formation and crustal recycling. *Tectonophysics*, **161**, 201–212.
- Beane, R.J. & Field, D.C.K., 2007. Kyanite deformation in whiteschist of the ultrahigh-pressure metamorphic Kokchetav

- Massif, Kazakhstan. *Journal of Metamorphic Geology*, **25**, 117–128.
- Birch, F., 1961. The velocity of compressional waves in rocks to 10 kilobar, Part 2. *Journal of Geophysical Research*, **66**, 2199–2224.
- Bird, P., 1978. Initiation of intracontinental subduction in the Himalaya. *Journal of Geophysical Research*, **83**, 4975–4987.
- Bird, P., 1979. Continental delamination and the Colorado Plateau. *Journal of Geophysical Research*, **84**, 7561–7571.
- Bostock, M.G., Hyndman, R.S., Rondenay, S. & Peacock, S.M., 2002. An inverted continental Moho and serpentinization of the forearc mantle. *Nature*, **417**, 536–539.
- Cammarano, F., Goes, S., Vacher, P. & Giardini, D., 2003. Inferring upper-mantle temperatures from seismic velocities. *Physics of the Earth and Planetary Interiors*, **138**, 197–222.
- Christensen, N.I., 1972. Abundance of serpentinites in oceanic crust. *Journal of Geology*, **80**, 709–719.
- Christensen, N.I., 1974. Compressional wave velocities in possible mantle rocks to pressures of 30 kilobars. *Journal of Geophysical Research*, **79**, 407–412.
- Christensen, N.I., 1985. Measurements of dynamic properties of rock at elevated temperatures and pressures. In: *Measurements of Rock Properties at Elevated Pressures and Temperatures* (eds Pincus, H.J. & Hoskins, E.R.), pp. 93–107. American Society for Testing and Materials, Philadelphia, PA.
- Christensen, N.I., 1996. Poisson's ratio and crustal seismology. *Journal of Geophysical Research*, **101**, 3139–3156.
- Christensen, N.I., 2004. Serpentinites, peridotites, and seismology. *International Geology Review*, **46**, 795–816.
- Comodi, P., Zanazzi, P.F., Poli, S. & Schmidt, M.W., 1997. High-pressure behavior of kyanite: compressibility and structure deformations. *American Mineralogist*, **82**, 452–459.
- Dill, H.G., 2007. A review of mineral resources in Malawi: with special reference to aluminium variation in mineral deposits. *Journal of African Earth Sciences*, **47**, 153–173.
- Dobson, D., Meredith, P.G. & Boon, S.A., 2002. Simulation of subduction zone seismicity by dehydration of serpentine. *Science*, **298**, 1407–1410.
- Doglioni, C., Carminati, E., Cuffaro, M. & Scrocca, D., 2007. Subduction kinematics and dynamic constraints. *Earth-Science Reviews*, **83**, 125–175.
- Ernst, W.G. & Liou, J.G., 2008. High- and ultrahigh-pressure metamorphism: past results and future prospects. *American Mineralogist*, **93**, 1771–1786.
- Fan, W.-M., Guo, F., Wang, Y.-J. & Zhang, M., 2004. Late Mesozoic volcanism in the northern Huaiyang tectono-magmatic belt, central China: partial melts from a lithospheric mantle with subducted continental crust relicts beneath the Dabie orogen? *Chemical Geology*, **209**, 27–48.
- Fischer-Cripps, A.C., 2000. *Introduction Contact Mechanics*, 1st edn. Springer-Verlag, New York, pp. 1–30.
- Gao, S., Kern, H., Jin, Z.M. *et al.*, 2001. Poisson's ratio of eclogite: the role of retrogression. *Earth and Planetary Science Letters*, **192**, 523–531.
- Gao, S., Rudnick, R.L., Yuan, H.-L. *et al.*, 2004. Recycling lower continental crust in the North China craton. *Nature*, **432**, 892–897.
- Gao, S., Rudnick, R.L., Xu, W.-L. *et al.*, 2008. Recycling deep cratonic lithosphere and generation of intraplate magmatism in the North China Craton. *Earth and Planetary Science Letters*, **270**, 41–53.
- Graham, E.K., Schwab, J.A., Sopkin, S.M. & Takei, H., 1988. The pressure and temperature dependence of the elastic properties of single-crystal fayalite Fe_2SiO_4 . *Physics and Chemistry of Minerals*, **16**, 186–198.
- Green, H.W., II, Dobrzhinetskaya, L., Riggs, E.M. & Jin, Z.-M., 1997. Alpe Arami: a peridotite massif from the Mantle Transition Zone? *Tectonophysics*, **279**, 1–21.
- Green, H.W., Dobrzhinetskaya, L. & Bozhilov, K.N., 2000. Mineralogical and experimental evidence for very deep exhumation from subduction zones. *Journal of geodynamics*, **30**, 61–76.
- Hacker, B.R., Peacock, S.M., Abers, G.A. & Holloway, S.D., 2003. Subduction factory, 2. Are intermediate-depth earthquakes in subducting slabs linked to metamorphic dehydration reactions? *Journal of Geophysical Research*, **108**(B1), 2030, doi: 10.1029/2001JB001129.
- Hess, H.H., 1959. The AmSoc hole to the earth's mantle. *Transactions of American Geophysical Union*, **40**, 340–345.
- Hess, H.H., 1962. History of the ocean basins. In: *Petrologic Studies: A Volume to Honor A.F. Buddington* (eds Engel, A.E.J., James, H.L., & Leonard, B.F.), pp. 599–620. Geological Society of America, Denver, CO.
- Higo, Y., Inoue, T., Irifune, T., Funakoshi, K.I. & Li, B., 2008. Elastic wave velocities of $(\text{Mg}_{0.91}\text{Fe}_{0.09})_2\text{SiO}_4$ ringwoodite under P-T conditions of the mantle transition region. *Physics of the Earth and Planetary Interiors*, **166**, 167–174.
- Hilaret, N., Reynard, B., Wang, Y. *et al.*, 2007. High-pressure creep of serpentine, interseismic deformation, and initiation of subduction. *Science*, **318**, 1910–1913.
- Huang, F., Li, S., Dong, F. *et al.*, 2007. Recycling of deeply subducted continental crust in the Dabie Mountains, central China. *Lithos*, **96**, 151–169.
- Hyndman, R.D. & Peacock, S.M., 2003. Serpentinization of the forearc mantle. *Earth and Planetary Science Letters*, **212**, 417–432.
- Irifune, T., Higo, Y., Inoue, T., Kono, Y., Ohfuji, H. & Funakoshi, K., 2008. Sound velocities of majorite garnet and the composition of the mantle transition region. *Nature*, **451**, 814–817.
- Isaak, D., Anderson, O., Goto, T. & Suzuki, I., 1989. Elasticity of single-crystal forsterite measured to 1700 K. *Journal of Geophysical Research*, **94**(B5), 5895–5906.
- Jahn, B.-M., Wu, F., Lo, C.-H. & Tsai, C.-H., 1999. Crust-mantle interaction induced by deep subduction of the continental crust: geochemical and Sr–Nd isotopic evidence from post-collisional mafic-ultramafic intrusions of the northern Dabie complex. *Chemical Geology*, **157**, 119–146.
- Jephcoat, A.P., 1998. Rare-gas solids in the Earth's deep interior. *Nature*, **393**, 355–358.
- Ji, S.C., Salisbury, M.H. & Hanmer, S., 1993. Petrofabric, P-wave anisotropy and seismic reflectivity of high-grade tectonites. *Tectonophysics*, **222**, 195–226.
- Ji, S.C., Wang, Z. & Saruwatari, K., 1998. Plasticity of eclogite: implications for rheology and seismic reflectivity of the subducting slab. In: *Proceedings of the LITHOPROBE Slave–Northern Cordillera Lithospheric Evolution (SNORCLE) and Cordilleran Tectonics Workshop: Burnaby, British Columbia, Simon Fraser University, LITHOPROBE Report 64*, pp. 86–91.
- Ji, S.C., Saruwatari, K., Mainprice, D., Wirth, R., Xu, Z.Q. & Xia, B., 2003. Microstructures, petrofabrics and seismic properties of ultrahigh-pressure eclogites from Sulu region, China: implications for rheology of subducted continental crust and origin of mantle reflections. *Tectonophysics*, **370**, 49–76.
- Ji, S.C., Wang, Q., Marcotte, D., Salisbury, M.H. & Xu, Z.Q., 2007. P-wave velocities, anisotropy and hysteresis in ultrahigh-pressure metamorphic rocks as a function of confining pressure. *Journal of Geophysical Research*, **112**, B09204, doi:10.1029/2006JB004867.
- Ji, S.C., Wang, Q. & Salisbury, M.H., 2009. Composition and tectonic evolution of the Chinese continental crust constrained by Poisson's ratio. *Tectonophysics*, **463**, 15–30.
- Jin, Z.-M., Zhang, J., Green, H.W. & Jin, S., 2001. Eclogite rheology: implications for subducted lithosphere. *Geology*, **29**, 667–670.
- Kawakatsu, H. & Watada, S., 2007. Seismic evidence for deep-water transportation in the mantle. *Science*, **316**, 1468–1471.
- Kay, R.W. & Kay, S.M., 1991. Creation and destruction of lower continental crust. *Geologische Rundschau*, **80**, 259–278.

- Kern, H. & Wenk, H.-R., 1990. Fabric related velocity anisotropy and shear wave splitting in rocks from the Santa Rosa mylonite zone, California. *Journal of Geophysical Research*, **95**, 11213–11223.
- Kern, H., Gao, S., Jin, Z.M., Popp, T. & Jin, S.Y., 1999. Petrophysical studies on rocks from the Dabie ultrahigh-pressure (UHP) metamorphic belt, central China: implications for the composition and delamination of the lower crust. *Tectonophysics*, **301**, 191–215.
- Kern, H., Jin, Z.M., Gao, S., Popp, T. & Xu, Z.Q., 2002. Physical properties of ultrahigh-pressure metamorphic rocks from the Sulu terrain, eastern central China: implications for the seismic structure at the Donghai (CCSD) drilling site. *Tectonophysics*, **354**, 315–330.
- Knoche, R., Webb, S.L. & Rubie, D.C., 1997. Experimental determination of acoustic wave velocity at Earth mantle conditions using a multivolt press. *Physics and Chemistry of the Earth*, **22**, 125–130.
- Li, B., Gwanmesia, G. & Liebermann, R., 1996. Sound velocities of olivine and beta polymorphs of Mg_2SiO_4 at Earth's transition zone pressures. *Geophysical Research Letters*, **23**, 2259–2262.
- Li, S., Nie, Y., Liu, D. & Zheng, Y., 1998a. Interaction between subducted continental crust and the mantle—I. Major and trace element geochemistry of the syncollisional mafic-ultramafic intrusions in the Dabie Mountains. *Science in China (D)*, **41**, 545–552.
- Li, S., Nie, Y., Hart, S.R. & Zhang, Z., 1998b. Interaction between subducted continental crust and the mantle—II. Sr and Nd isotopic geochemistry of the syncollisional mafic-ultramafic intrusions in Dabie Mountains. *Science in China (D)*, **41**, 632–638.
- Li, S., Huang, F. & Li, H., 2002. Post-collisional lithosphere delamination of the Dabie–Sulu orogen. *Chinese Science Bulletin*, **47**, 259–263.
- Liou, J.G., Maruyama, S. & Ernst, W.G., 1997. Seeing a mountain in a grain of garnet. *Science*, **276**, 48–49.
- Liou, J.G., Ernst, W.G., Zhang, R.Y., Tsujimori, T. & Jahn, B.-M., 2009. Ultrahigh-pressure minerals and metamorphic terranes—the view from China. *Journal of Asian Earth Sciences*, **35**, 199–231.
- Liu, Y., Gao, S., Kelemen, P.B. & Xu, W., 2008. Recycled crust controls contrasting source compositions of Mesozoic and Cenozoic basalts in the North China Craton. *Geochimica et Cosmochimica Acta*, **72**, 2349–2376.
- Liu, X., Shieh, S.R., Fleet, M.E. & Zhang, L., 2009. Compressibility of a natural kyanite to 17.5 GPa. *Progress in Natural Science*, **19**, 1281–1286.
- Ma, C., Li, Z., Ehlers, C., Yang, K. & Wang, R., 1998. A post-collisional magmatic plumbing system: Mesozoic granitoid plutons from the Dabieshan high-pressure and ultrahigh-pressure metamorphic zone, east-central China. *Lithos*, **45**, 431–456.
- Massonne, H.-J., Willner, A.P. & Gerya, T., 2007. Densities of metapelitic rocks at high to ultrahigh pressure conditions: what are the geodynamic consequences? *Earth and Planetary Science Letters*, **256**, 12–27.
- Matsushima, S., 1972. Compressional wave velocity in olivine nodules at high pressure and temperature. *Journal of Physics of the Earth*, **20**, 187–195.
- Mikowski, A., Soares, P., Wypych, F. & Lepienski, C.M., 2008. Fracture toughness, hardness, and elastic modulus of kyanite investigated by a depth-sensing indentation technique. *American Mineralogist*, **93**, 844–852.
- Moore, V.M. & Wiltshko, D.V., 2004. Syncollisional delamination and tectonic wedge development in convergent orogens. *Tectonics*, **23**, TC2005, doi:10.1029/2002TC001430.
- Niu, Y., 2004. Bulk-rock major and trace element compositions of abyssal peridotites: implications for mantle melting, melt extraction and post-melting processes beneath ocean ridges. *Journal of Petrology*, **45**, 2423–2458.
- Niu, Y.L., 2005. Generation and evolution of basaltic magmas: some basic concepts and a hypothesis for the origin of the Mesozoic-Cenozoic volcanism in eastern China. *Geological Journal of China Universities*, **11**, 9–46.
- Niu, Y. & Batiza, R., 1991. In-situ densities of silicate melts and minerals as a function of temperature, pressure, and composition. *Journal of Geology*, **99**, 767–775.
- Okay, A.I., Xu, S.-T. & Sengor, A.M.C., 1989. Coesite from the Dabie Shan eclogites, central China. *European Journal of Mineralogy*, **1**, 595–598.
- Peacock, S.M., 2001. Are the lower planes of double seismic zones caused by serpentine dehydration in subducting oceanic mantle? *Geology*, **29**, 299–302.
- Rapp, R.P., Irifune, T., Shimizu, N., Nishiyama, N., Norman, M.D. & Inoue, T., 2008. Subduction recycling of continental sediments and the origin of geochemically enriched reservoirs in the deep mantle. *Earth and Planetary Science Letters*, **271**, 14–23.
- Ren, Y. & Shen, Y., 2008. Finite frequency tomography in southeastern Tibet: evidence for the causal relationship between mantle lithosphere delamination and the north–south trending rifts. *Journal of Geophysical Research*, **113**, B10316, doi:10.1029/2008JB005615.
- Sinogeikin, S.V. & Bass, J.D., 2002. Elasticity of pyrope and majorite-pyrope solid solutions to high temperatures. *Earth and Planetary Science Letters*, **203**, 549–555.
- Song, S., Zhang, L., Niu, Y., Su, L., Jian, P. & Liu, D., 2005. Geochronology of diamond-bearing zircons in garnet-peridotite in the North Qaidam UHPM belt, North Tibetan Plateau: a record of complex histories associated with continental collision. *Earth and Planetary Science Letters*, **234**, 99–118.
- Spetsius, Z.V., 2004. Petrology of highly aluminous xenoliths from kimberlites of Yakutia. *Lithos*, **77**, 525–538.
- Sumino, Y., 1979. The elastic constants of Mn_2SiO_4 , Fe_2SiO_4 and Co_2SiO_4 , and the elastic properties of olivine group minerals at high temperature. *Journal of Physics of the Earth*, **27**, 209–238.
- Suzuki, I., Anderson, O.L. & Sumino, Y., 1983. Elastic properties of a single-crystal forsterite Mg_2SiO_4 , up to 1200 K. *Physics and Chemistry of Minerals*, **10**, 38–46.
- Wang, Z. & Ji, S., 1999. Deformation of silicate garnets: brittle-ductile transition and its geological implications. *Canadian Mineralogist*, **37**, 525–541.
- Wang, X., Liou, J.G. & Mao, H.K., 1989. Coesite-bearing eclogite from the Dabie Mountains in central China. *Geology*, **17**, 1085–1088.
- Wang, C.-Y., Ding, Z.-F., Song, J.-L., Wu, Q.-Z., Zhen, J.C. & Zhang, X.-B., 1997. Shear wave velocity structure of the Dabie orogenic belt. *Acta Geophysica Sinica*, **40**, 337–345.
- Wang, C.Y., Zeng, R.S., Mooney, W.D. & Hacker, B.R., 2000. A crustal model of the ultrahigh-pressure Dabie Shan orogenic belt, China, derived from deep seismic refraction profiling. *Journal of Geophysical Research*, **105**, 10857–10869.
- Wang, Q., Ji, S.C., Salisbury, M.H., Pan, M.B., Xia, B. & Xu, Z.Q., 2005a. Pressure dependence and anisotropy of P-wave velocities in ultrahigh-pressure metamorphic rocks from the Dabie–Sulu orogenic belt (China): implications for seismic properties of subducted slabs and origin of mantle reflections. *Tectonophysics*, **398**, 67–99.
- Wang, Q., Ji, S.C., Salisbury, M.H., Xia, B., Pan, M.B. & Xu, Z.Q., 2005b. Shear wave properties and Poisson's ratios of ultrahigh-pressure metamorphic rocks from the Dabie–Sulu orogenic belt: implications for the crustal composition. *Journal of Geophysical Research*, **110**, B08208, doi:10.1029/2004JB003435.
- Wang, Y., Fan, W., Peng, T., Zhang, H. & Guo, F., 2005c. Nature of the Mesozoic lithospheric mantle and tectonic decoupling beneath the Dabie Orogen, central China: evidence from $^{40}Ar/^{39}Ar$ geochronology, elemental and Sr–Nd–Pb isotopic compositions of early Cretaceous mafic igneous rocks. *Chemical Geology*, **220**, 165–189.

- Wang, Q., Burlini, L., Mainprice, D. & Xu, Z., 2009. Geochemistry, petrofabrics and seismic properties of eclogites from the Chinese Continental Scientific Drilling boreholes in the Sulu UHP terrane, eastern China. *Tectonophysics*, **475**, 251–266.
- Wang, L., Jin, Z.M., Kusky, T., Xu, H.L. & Liu, X.W., 2010. Microfabric characteristics and rheological significance of ultra-high-pressure metamorphosed jadeite-quartzite and eclogite from Shuanghe, Dabie Mountains, China. *Journal of Metamorphic Geology*, **28**, 163–182.
- Whitney, D.L., Broz, M. & Cook, R.F., 2007. Hardness, toughness, and modulus of some common metamorphic minerals. *American Mineralogist*, **92**, 281–288.
- Winkler, B., Hytha, M., Warren, C.M., Milman, V., Gale, J.D. & Schreuer, J., 2001. Calculation of the elastic constants of the Al_2SiO_5 polymorphs andalusite, sillimanite, and kyanite. *Zeitschrift für Kristallographie*, **216**, 67–70.
- Wu, Y., Fei, Y., Jin, Z. & Liu, X., 2009. The fate of subducted upper continental crust: an experimental study. *Earth and Planetary Science Letters*, **282**, 275–284.
- Xu, S.T., Okay, A.L., Ji, S. *et al.*, 1992. Diamond from the Dabie Shan metamorphic rocks and its implication for tectonic setting. *Science*, **256**, 80–82.
- Xu, P.F., Liu, F.T., Wang, Q.C., Cong, B.L. & Chen, H., 2001. Slab-like high velocity anomaly in the upper most mantle beneath Dabie–Sulu orogen. *Geophysical Research Letters*, **28**, 1847–1850.
- Yang, W., 2009. The crust and upper mantle of the Sulu UHPM belt. *Tectonophysics*, **475**, 226–234.
- Yang, J.-J., Godard, G., Kienast, J.-R., Lu, Y. & Sun, J., 1993. Ultrahigh-pressure (60 kbar) magnesite-bearing garnet peridotites from northeastern Jiangsu. *Journal of Geology*, **101**, 541–554.
- Yang, H., Downs, R.T., Finger, L.W., Hazen, R.M. & Prewitt, C.T., 1997a. Compressibility and crystal structure of kyanite, Al_2SiO_5 , at high pressure. *American Mineralogist*, **81**, 467–474.
- Yang, H., Hazen, R.M., Downs, R.T., Finger, L.W. & Prewitt, C.T., 1997b. Compressibility and crystal structure of sillimanite, Al_2SiO_5 , at high pressure. *Physics and Chemistry of Minerals*, **25**, 39–47.
- Ye, K., Cong, B. & Ye, D., 2000. The possible subduction of continental material to depths greater than 200 km. *Nature*, **407**, 734–736.
- You, Z., Han, Y., Yang, W., Zhang, Z. & Wei, B., 1996. *The High-pressure and Ultra-high-pressure Metamorphic Belt in the East Qinling and Dabie mountains, China*. China University of Geosciences Press, Wuhan, pp. 150.
- Zaug, J.M., Abramson, E.H., Brown, J.M. & Slutsky, L.J., 1993. Sound wave velocity in olivine at Earth mantle pressures. *Science*, **260**, 1487–1490.
- Zhang, Z.-M., Xu, Z.-Q. & Xu, H.-F., 2000. Petrology of ultrahigh-pressure eclogites from the ZK703 drillhole in the Donghai, eastern China. *Lithos*, **52**, 35–50.
- Zhang, H.-F., Sun, M., Zhou, M.-F., Fan, W.-M., Zhou, X.-H. & Zhai, M.-G., 2004. Highly heterogeneous Late Mesozoic lithospheric mantle beneath the North China craton: evidence from Sr–Nd–Pb isotopic systematics of mafic igneous rocks. *Geological Magazine*, **141**, 55–62.
- Zhang, G.B., Song, S.G., Zhang, L.F. & Niu, Y., 2008. The subducted oceanic crust within continental-type UHP metamorphic belt in the North Qaidam, NW China: evidence from petrology, geochemistry and geochronology. *Lithos*, **104**, 99–118.
- Zhao, D., 2004. Global tomographic images of mantle plumes and subducting slabs: insight into deep earth dynamics. *Physics of the Earth and Planetary Interiors*, **146**, 3–34.
- Zhao, Z., Xie, H., Zhou, W. *et al.*, 1998. Compressional wave velocities in eclogites of the Dabieshan, central China to 5.0 GPa: a Preliminary Result. *The Review of High Pressure Science and Technology*, **7**, 12–14.
- Zhao, Z., Zhou, W., Xie, H., Guo, J., Xu, Z. & Zhang, Z., 1999. P-wave velocity in rocks of Dabieshan, China at high pressure and high temperature: constraints for the composition of the lower crust and crust–mantle recycling. *Journal of China University of Geosciences*, **10**, 295–298.
- Zhao, Z.-F., Zheng, Y.-F., Wei, C.-S., Wu, Y.-B., Chen, F.-K. & Jahn, B.-M., 2005. Zircon U–Pb age, element and C–O isotope geochemistry of post-collisional mafic–ultramafic rocks from the Dabie orogen in east-central China. *Lithos*, **83**, 1–28.
- Zheng, Y.-F., Fu, B., Gong, B. & Li, L., 2003. Stable isotope geochemistry of ultrahigh-pressure metamorphic rocks from the Dabie–Sulu orogen in China: Implications for geodynamics and fluid regime. *Earth-Science Review*, **62**, 105–161.

Received 12 February 2010; revision accepted 9 March 2011.